

# EUMETSAT/ECMWF Fellowship Programme Research Report

# 59

## All-sky Assimilation of AMSU-A Window Channels

David I. Duncan, Niels Bormann, Alan J. Geer

Aug 2022

Series: EUMETSAT/ECMWF Fellowship Programme Research Reports

A full list of ECMWF Publications can be found on our web site under:

<http://www.ecmwf.int/en/publications/>

Contact: [library@ecmwf.int](mailto:library@ecmwf.int)

© Copyright 2022

European Centre for Medium Range Weather Forecasts, Shinfield Park, Reading, RG2 9AX, UK

Literary and scientific copyrights belong to ECMWF and are reserved in all countries. The content of this document is available for use under a Creative Commons Attribution 4.0 International Public License.

See the terms at <https://creativecommons.org/licenses/by/4.0/>.

The information within this publication is given in good faith and considered to be true, but ECMWF accepts no liability for error or omission or for loss or damage arising from its use.

## Abstract

Following the activation of AMSU-A temperature sounding channels in all-sky conditions at ECMWF, here we consider assimilation of its window channels. These frequencies hold information on clouds and precipitation, columnar water vapour, and low-level winds in 4D-Var, but at ECMWF such channels have previously been assimilated on conically-scanning microwave imagers only. Suitable error modelling is investigated for these channels, with their different sensitivities requiring predictors separate from the sounding channels. In comparison to sounding channels on AMSU-A or similar frequencies on conically-scanning imagers, all-sky error modelling for these channels is more challenging. This is primarily due to their combination of sensitivities to the surface and scattering from hydrometeors aloft in clouds and precipitation that changes with the variable zenith angle.

All-sky assimilation of the AMSU-A window channels is shown to be similar to that of microwave imagers when adequate quality control and observation error modelling are applied; different observation error models are tested, with a 50 GHz-based cloud proxy yielding the best results. The choice of observation error model has a modest effect on the assimilation, though smaller than that of the additional data itself. Experiments using a depleted observing system indicate that active use of these window channels can impart a good fraction of the impact provided by four microwave imagers. When compared to a full observing system, the addition of AMSU-A window channels provides a small but significant improvement in background fits to observations of winds and humidity. These benefits are most notable in the tropics, where the addition of AMSU-A window channels fills in temporal sampling gaps left by the imagers. Signals in the analysis-based verification are small and more mixed, with improvement seen for columnar humidity in the tropics out to day 2 but degradation of low-level temperature forecasts in the southern hemisphere out to day 4. Further testing will be performed to ascertain the suitability of assimilating the AMSU-A window channels in a future operational cycle.

## Plain Language Summary

Satellite sensors that were built for atmospheric sounding—sensing vertical profiles of temperature and/or humidity—also typically hold channels with primary sensitivity to clouds, precipitation, and the earth’s surface for the purpose of screening. These channel frequencies have previously been used to improve weather forecasts when assimilated from other, purpose-built sensors, so here we explore actively assimilating these channels from the microwave sounder AMSU-A. This is in line with a larger strategy of exploiting satellite radiances as much as possible to benefit weather forecasting, in this case by assimilating radiances that were previously discarded. The results show that addition of these channels does improve short-range forecasts of humidity and winds, however some further work may be necessary to make this development ready for activation in the operational system.

## 1 Introduction

Microwave temperature sounding instruments such as the Advanced Microwave Sounding Unit-A (AMSU-A) possess non-sounding channels in so-called “window” regions of the spectrum. These channels have greater sensitivity to cloud and surface parameters than sounding channels, whose sensitivity peaks above the surface for profiling gaseous species. Window channels can hold useful ancillary information for screening or retrieving parameters for which the sounding channels may have secondary sensitivity. In the case of assimilating AMSU-A channels 5-9, at ECMWF the channels 1 and 2 are used to retrieve line-of-sight liquid water path (LWP) over sea to inform the all-sky error model; similarly,

Table 1: Channels on AMSU-A are given by number, centre frequency in GHz, and peak of the weighting function in pressure. Channels' peak sensitivity is given as the approximate pressure range of the weighting function maximum from nadir to scan edge. Sounding channels 6 through 14 are omitted here.

Channel	Frequency [GHz]	Peak sensitivity [hPa]
1	23.8	Surface
2	31.4	Surface
3	50.3	Surface
4	52.8	920 - 810
5	53.596±0.115	650 - 530
15	89.0	Surface

over land channels 1 and 15 form a scattering index (SI) that informs the error model (Duncan *et al.*, 2022). Channel 3 powers the dynamic emissivity retrieval over land surfaces.

In this paper we explore expanding the use of window channels beyond that of error modelling for sounder channels to full active assimilation in the ECMWF Integrated Forecasting System (IFS).

## 1.1 Background

The microwave spectrum is relatively transparent through much of the Earth's atmosphere. Notable exceptions to this exist: between 50 to 60 GHz where numerous strong absorption features from molecular oxygen make the atmosphere mostly opaque; near a strong oxygen absorption line at 118.75 GHz; and near 183.31 GHz where a strong water vapour absorption line sits. Water vapour continuum absorption also makes the atmosphere increasingly opaque as frequency increases. These absorption features can be exploited for atmospheric sounding of temperature and humidity. This leaves several spectral regions of greater transparency that function instead to provide information on Earth's surface properties and atmospheric species such as precipitation, liquid cloud drops, or frozen particles that increase or decrease observed radiances via emission or scattering of microwaves, respectively.

Microwave sounders typically hold a suite of sounding channels in one or several of these regions of strong atmospheric emission to profile temperature and/or humidity. AMSU-A channels 4-14 exploit oxygen emission features between 50 to 60 GHz, whereas sensors such as the Microwave Humidity Sounder (MHS) exploit water vapour emission. Channel 4 on AMSU-A is primarily a sounding channel but has significant surface sensitivity and is not yet assimilated operationally (see Appendix B). Most sounding sensors hold window channels as well, ostensibly to guide the use of these sounding channels in retrievals or data assimilation. For example, both AMSU-A and MHS have a channel at 89 GHz, a window frequency with strong sensitivity to precipitation, clouds, and surface properties. AMSU-A in particular holds four window channels at 23.8, 31.4, 50.3, and 89 GHz, as seen in Table 1; in this paper we will primarily refer to these by their channel numbers.

The window channels on AMSU-A have distinct properties in addition to surface sensitivity. Channels 1 and 2 have similar sensitivities, primarily to cloud water and precipitation. Channel 1 however lies near a water vapour absorption line at 22.235 GHz, and thus the difference of channels 1 and 2 can yield information on columnar water vapour as well as cloud water, a "split-window" retrieval approach (e.g. Grody *et al.*, 2001). Channel 3 sits in a window region but is nearby the main sounding channels in frequency space, meaning that it is useful for sensing the surface properties that have secondary effects on sounding channel radiances; it also holds numerous atmospheric sensitivities including liquid and

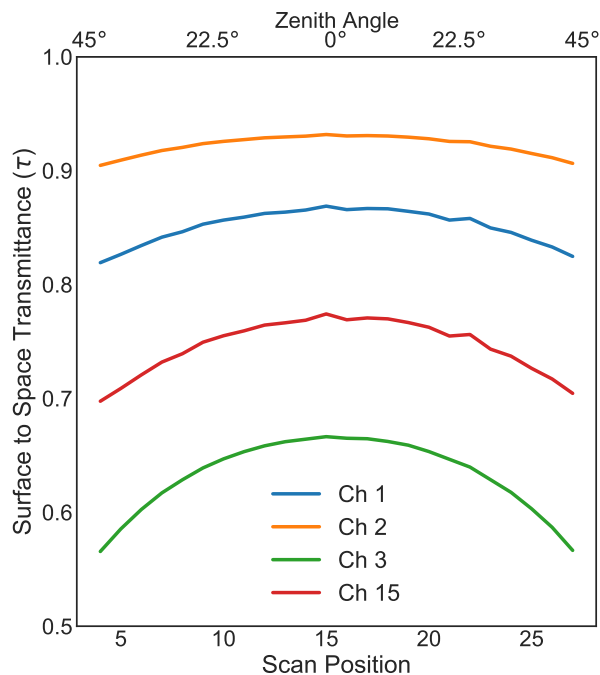


Figure 1: Mean surface to space transmittance as a function of scan position and zenith angle for AMSU-A window channels, shown from operational all-sky Metop-C data over sea on December 28th, 2021. Scan positions 1-3 and 28-30 are excluded in the IFS and thus not shown.

frozen hydrometeors, water vapour continuum emission, and oxygen emission. In the IFS, the mean surface to space transmittance ( $\tau$ ; essentially surface sensitivity) of channel 3 over sea is about 0.6. So although channel 3 is mainly a surface-sensitive channel, it can be considered a pseudo-sounding channel particularly near the scan edge (see Fig. 1). Lastly, channel 15 is the highest frequency channel on AMSU-A and thus holds the greatest sensitivity to scattering from frozen and liquid hydrometeors. Channel 15 has sensitivity to cloud and precipitation properties, but like channel 3 it holds some non-negligible information on atmospheric gas emission with  $\tau \approx 0.75$  mean value and significant variability due to water vapour.

## 1.2 Window channel assimilation

Exploiting microwave window frequencies in data assimilation to benefit numerical weather prediction (NWP) is hardly a novel concept. Direct all-sky assimilation of window channel radiances has been operational at ECMWF for over a decade (Bauer *et al.*, 2010), providing unique information on water vapour and clouds in the lower troposphere due to microwaves' relative transparency through cirrus clouds. As of early 2022 at ECMWF, four conically-scanning microwave imagers are actively assimilated at frequencies spanning 19 to 91 GHz: GMI (the Global Precipitation Measurement (GPM) Microwave Imager), SSMIS (Special Sensor Microwave Imager/Sounder) on DMSP F17, AMSR2 (Advanced Microwave Scanning Radiometer-2), and MWRI (Microwave Radiation Imager) on FY-3D. For details on which imager channels are assimilated and over which surfaces, see Geer *et al.* (2022) and their Table 1. In the USA at NCEP (National Centers for Environmental Prediction), window channels on AMSU-A and the Advanced Technology Microwave Sounder (ATMS) are already assimilated operationally (Zhu *et al.*, 2019), albeit with strict quality control to avoid scattering.

It is useful to put the AMSU-A window channels into context relative to the microwave imagers assimilated. As of early 2022 there are five AMSU-A sensors actively used in all-sky conditions within the IFS: Metop-B, Metop-C, NOAA-15, NOAA-18, and NOAA-19 (Metop-A deorbited in Nov. 2021). All these sensors have working channels 1, 2, and 15 with the exception of Metop-B, whose channel 15 broke in 2016. This adds up to 14 potential window channels to assimilate at 23.8, 31.4, and 89 GHz. These all measure a single polarisation per frequency, whereas most microwave imagers hold both vertical (V) and horizontal (H) polarisation channels to best exploit their observation near the Brewster angle. The sum total of traditional imager channels (i.e. channels near 19, 24, 36, and 89 GHz) used in the IFS is currently 22 from four sensors. So to put this into perspective, the AMSU-A window channels are akin to perhaps two additional microwave imagers but split across 5 sun-synchronous polar orbits. This may hold distinct benefit for constraining the fast-changing fields of clouds and precipitation, particularly in the tropics where sampling from polar-orbiting sensors is sparsest.

Assimilation of additional microwave sounders adds to forecast skill for global NWP in the short- to medium-range (Duncan *et al.*, 2021). Furthermore, future constellations of small satellites intend to provide higher temporal resolution of atmospheric sounding observations, for instance in the tropics (Blackwell *et al.*, 2018). Here we attempt to do similarly but by using existing and mature technology that is already well characterised and providing significant positive impact in the all-sky framework (Duncan *et al.*, 2022). Scattering simulation has recently improved with the upgrade of radiative transfer modelling to RTTOV-SCATT v13 (Geer *et al.*, 2021). Previous issues with lower tropospheric drying in the IFS due to additional microwave imager radiances have been largely resolved (Lonitz and Geer, 2020), spurring on activation of MWRI in May 2020 as the fourth imager assimilated (Bormann *et al.*, 2021). Lastly, the latest IFS upgrade to Cycle 48r1 contains a suite of changes to all-sky radiance usage including increased window channel use over higher latitudes, coastal regions, and land, showing a neutral to positive impact from significantly more radiances assimilated (Geer *et al.*, 2022); these are mostly not applicable to AMSU-A window channels, but indicative of continued expansion of all-sky MW usage and the possible benefits. The confluence of these factors indicates that the system may now be primed to benefit from additional window channel radiances.

## 2 Methods

### 2.1 Observation Error Modelling

The observation-error modelling for all-sky assimilation is underpinned by a symmetric predictor of total error that is used to capture larger errors in areas of cloud and precipitation (Geer and Bauer, 2011). For imagers, the error model is driven by a normalised polarisation difference near 37 GHz (P37), a good indicator of emission and scattering within the satellite field of view. This works for conically-scanning radiometers due to their near-constant viewing geometry near the Brewster angle of about 55 degrees, where surface emissivity differences between V and H polarisations maximise over sea and provide high contrast for atmospheric signals. With a variable zenith angle of observation, cross-track instruments such as AMSU-A do not possess dual-polarised channels and therefore other cloud indicators are needed. For all-sky AMSU-A sounding channels 5 to 9, an estimate of the liquid-water path (LWP) and a scattering index (SI) are derived from window channels 1, 2, and 15 to power the error model over sea and land, respectively (Duncan *et al.*, 2022).

Whereas channels 5 and 6 have primary sensitivity to the mid troposphere and liquid clouds, the window channels see deeper into the troposphere where scattering from graupel and rain hydrometeors some-

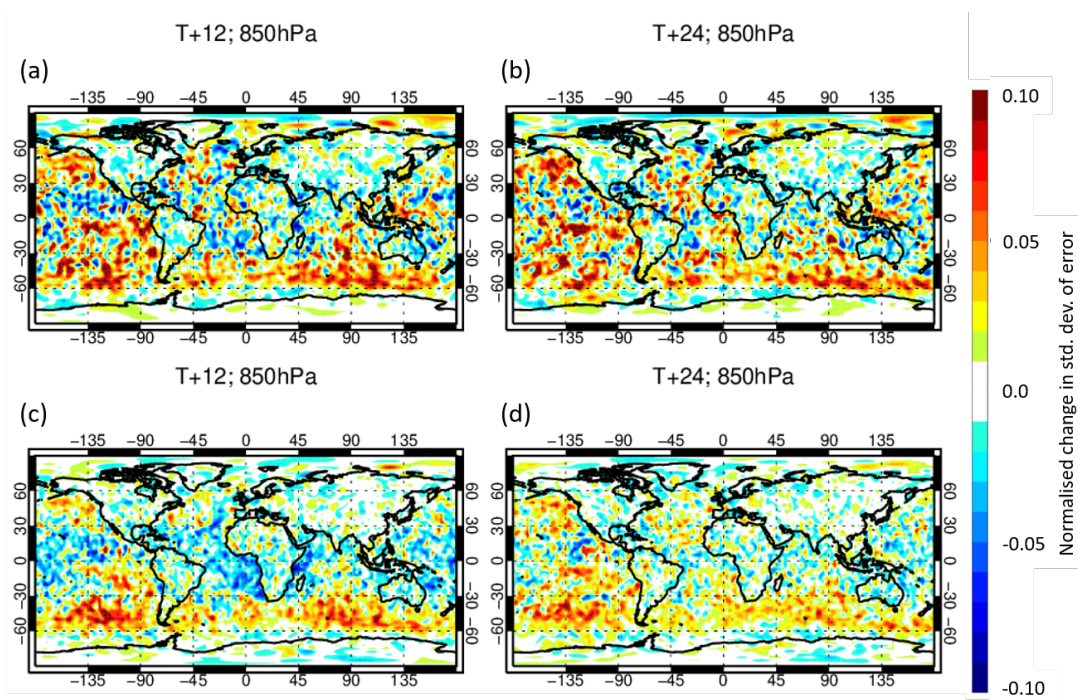


Figure 2: Change in standard deviation of forecast error at T+12 and T+24 for temperature (a,b) and relative humidity (c,d) at 850 hPa from adding assimilation of AMSU-A 1/2/15 with LWP-based errors to the full observing system. Verification is against own analysis and experimentation spans 6 months.

times dominate the atmospheric signal. Furthermore, while most sounding channels have limited surface sensitivity, emissivity errors can have a large impact on window channel radiances. The imagers' P37 can indicate emissivity errors implicitly as some emissivity errors are manifest in polarisation differences, but by design LWP and SI do not contain emissivity information. For these reasons it is worth considering what the optimal error predictor may be for AMSU-A window channel assimilation; this type of analysis is also important for future sensors that lack the channels needed for LWP retrieval such as on proposed small platform constellations (Lean *et al.*, 2022).

Early experimentation started with a LWP-based error model over ocean, following the example of the sounder channels. Despite many encouraging signs, assimilation of all three window channels caused significant degradation of scores at low levels, particularly in the southern ocean. This can be seen in Fig. 2, with own-analysis temperature and humidity errors increasing at 850 hPa primarily over the extratropical oceans; such signals are common for all-sky assimilation when the field variability (spatial standard deviation) also increases due to a “noisier” analysis, but in this case the field variability was unchanged and so this seems to be a real concern. Window channel assimilation is beneficial to humidity forecasts at short range in the tropics, but 5-10% degradation is seen in much of the southern ocean and north Pacific. There was also a slightly degraded fit to atmospheric motion vector (AMV) observations in the southern hemisphere, indicating that wind forecasts were also adversely affected.

In addition, stratocumulus regions west of South America suffered degraded forecasts at lower levels, a signal consistent with some previous experience of assimilating imager radiances (Lonitz and Geer, 2017) but of stronger magnitude. A key early finding was that poor results were driven by negative background departures, primarily from channel 15, indicating that scattering scenes were the main problem. In contrast to the LWP-based results, testing with a SI-based error model predictably performed even worse for regions dominated by low cloud that is mostly non-scattering (not shown). Clearly the error

modelling for these channels needs to account for emission from liquid cloud as well as scattering from convective clouds and precipitation. This testing led to consideration of two options: a combination of LWP and SI, and a predictor based at 50GHz.

Correlated error is one aspect of all-sky observation error modelling that is typically neglected and indeed it is neglected in the approaches here. For microwave window channels, background departures can be highly correlated between channels, and spatial correlations are also non-negligible, with a strong dependence whether a scene is cloudy or clear (Bormann *et al.*, 2011). And although ocean emissivity modelling is much more accurate than that over land, errors over sea are not negligible, particularly when it comes to the skin temperature used, belying the current lack of strong coupling in the IFS. It may be important to consider the impact of surface-related and correlated contributions to total observation error. For instance, the cross-scan geometry of sounding sensors means that there is greater surface sensitivity than encountered by conical scanners, as near-nadir radiances from AMSU-A channel 15 are about 20% more surface-sensitive than the same frequency on an imager. Emissivity errors could thus play a larger role in the total error for window channels on sounders. For these reasons, error modelling for cloudy scenes is inflated here relative to  $\text{std}(O-B)$  for an implicit accounting of correlated errors, and one of the predictors tested below implicitly accounts for surface errors by using departures from a surface-sensitive channel. This is to say that until correlated errors are dealt with more comprehensively (e.g. Duncan *et al.*, 2018; Weston and Bormann, 2018; Schulte and Kummerow, 2019), the limited nature of the diagonal error modelling applied here needs to be kept in mind.

### 2.1.1 LWP and SI

The line-of-sight LWP retrieval used presently in the all-sky AMSU-A assimilation is defined as in Geer *et al.* (2012), using the brightness temperatures (TB) from channels 1 and 2 and a function of the zenith angle ( $\theta$ ):

$$LWP = 8.24 - \cos(\theta)(2.539 - 1.744\cos(\theta)) + 0.754\ln(285 - TB_1) - 2.265\ln(285 - TB_2). \quad (1)$$

The “symmetric” cloud indicator of Geer and Bauer (2011),  $C$ , is formed by balancing the observed LWP with the model-predicted (i.e. background) LWP from simulated TBs:

$$C_{LWP} = (LWP_{obs} + LWP_{FG})/2 \quad (2)$$

An example of the LWP retrievals is seen in Fig. 3(b) for a 12-hour period.

The disadvantage of using LWP by itself as the error predictor is that it lacks sensitivity to frozen hydrometeors, a key source of error for window channels in tropical deep convection and frontal precipitation in midlatitudes. A possible solution is to augment the LWP error model with a term sensitive to scattering. The SI is a suitable proxy that exploits the general increase of scattering signal with frequency. For AMSU-A sounder channels over land, a simple SI formulation suffices (where  $B$  is the all-sky background radiance):

$$C_{SI, simple} = ((O_1 - O_{15}) + (B_1 - B_{15}))/2 \quad (3)$$

Over sea, however, differences in emissivity and water vapour absorption between the 23.8 and 89 GHz channels are much more significant—discrepancies as large as 50 or 60K. To circumvent this issue for

humidity sounders, [Geer et al. \(2014\)](#) proposed the “ocean SI,” which subtracts out the clear-sky difference between the two channels to better isolate the scattering signal from hydrometeors:

$$C_{SI} = ((O_1 - O_{15}) + (B_1 - B_{15}))/2 - (B_{clr,1} - B_{clr,15}) \quad (4)$$

This formulation ties SI closer to actual scattering signals for these frequencies, but an issue remains—channel 15 is much more sensitive to liquid water emission than channel 1, meaning that SI is strongly negative in regions dominated by liquid cloud. The differential signal between cloudy regions of mostly frozen and liquid cloud water is stark in Fig. 3(a), with small areas of positive SI mostly in the tropics whilst the extratropics are mostly negative due to predominant liquid clouds. Unlike for sounding channels over land ([Duncan et al., 2022](#), Fig. 2), negative SI in this case does have some correlation with departures. Furthermore, we would like to avoid treating SI with an absolute value in the error model, as the positive and negative values indicate different types and signs of errors for the window channels; indeed this approach would likely underestimate errors for scenes in which the emission and scattering signals are of similar magnitude.

Instead, we aim to combine the sensitivities of the LWP retrieval with the better-formulated SI (Eq. 4), so as to account for emitting and scattering hydrometeors together. In this paper we will use a crude formula with a nominal term to balance LWP and SI contributions to the error model. An offline analysis found that  $\text{std}(O-B)$  for channels 1 and 2 was roughly similar for  $SI \approx 30K$  and  $LWP \approx 1mm$ , so the formula for the combined LWP and SI weights them thus. The formula is additive so as to not cancel out one signal with the other, and ignores negative SI as LWP is deemed more meaningful for cloud emission.

$$C_{LWP+SI} = C_{LWP} + \max(0, C_{SI}/30.0) \quad (5)$$

This particular combination of LWP and SI has not been optimised, and a more sophisticated model could perhaps perform better. However, Eq. 5 should succeed at augmenting the LWP-based model by downweighting observations in regions of significant scattering by frozen hydrometeors. Comparison of panels (b) and (c) in Fig. 3 shows that the overall picture does not change much when adding SI on top of LWP, but that regions of heavy precipitation and deep convection will receive less weight in the analysis.

### 2.1.2 Predictor Based on Channel 3

As seen in Table 1, channel 3 sits amidst channels 1, 2, and 15 in frequency space and thus holds some combination of these frequencies’ sensitivities to liquid and frozen hydrometeors, plus significant surface sensitivity (Fig. 1). However, a simple departure-based error model (e.g. using  $|O - B|$  alone) would not capture the important case in which the observation and the model both have cloud present. To use the sensitivities of channel 3 to advantage, whilst retaining the symmetric nature of the all-sky error model, we formulate the error predictor ( $C$ ) thus:

$$C_{Ch3} = |O_3 - B_{3,clr}|/2 + |B_3 - B_{3,clr}|/2 \quad (6)$$

Here  $B_{clr}$  is the background radiance from RTTOV-SCATT with no hydrometeors present (i.e. gaseous emission only) while  $B$  is the full background radiance including contributions from liquid and frozen hydrometeors. Following the symmetric predictor of [Geer and Bauer \(2011\)](#), there are two equally weighted halves in this formulation. In the classic all-sky error model, half is essentially driven by

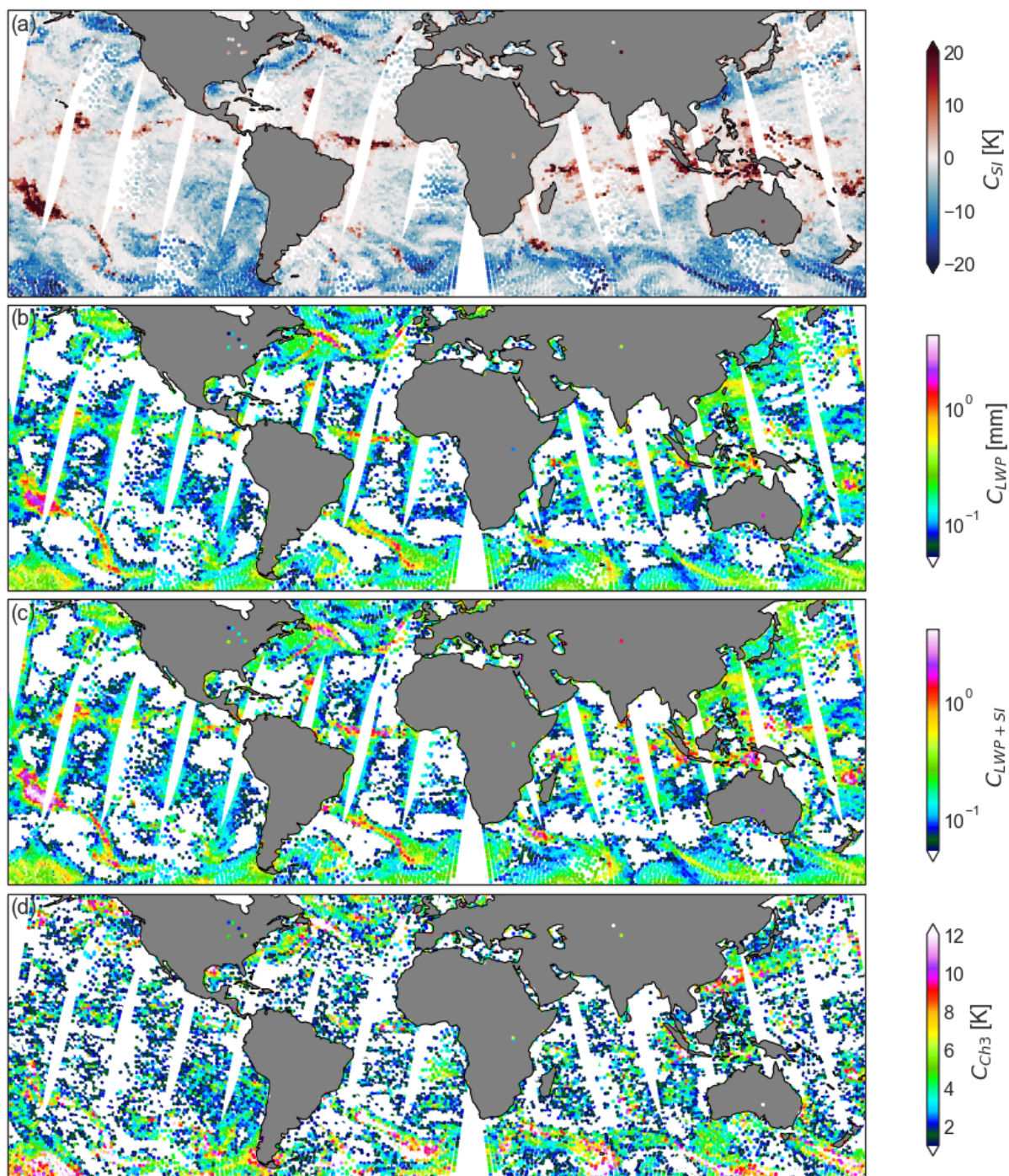


Figure 3: Four potential error model predictors for AMSU-A window channels: scattering index (a), liquid water path (b), a combination of LWP and SI (c), and channel 3-based (d). Data are from Metop-C on December 15, 2020 for the 12Z window, encompassing all available observations over sea.

whether the observed radiances see cloud, and the other half whether the modelled radiances see cloud. One half of Eq. 6 measures the presence of radiometrically significant cloud or precipitation in the model background ( $B - B_{clr}$ ). The other side ( $O - B_{clr}$ ) measures whether the observed radiance deviates from the modelled clear-sky atmosphere, which may include contributions from emissivity, water vapour, or

temperature profile errors. In this subtle way, the above predictor contains more information on whether cloud is present and on observation/model mismatch than a simple departure. A similar predictor has been successfully adopted by [Lean \*et al.\* \(2022\)](#) for all-sky assimilation of potential future 50-GHz temperature-sounders that lack channels needed for the LWP retrieval (using channel 4 instead).

Figure 3(d) shows a map of the  $C_{Ch3}$  for Metop-C. The main features here appear to be clouds—we can see regions of frontal cloud at higher latitudes, tropical convection, likely evidence of stratocumulus clouds west of Chile, and so on. Particularly striking is that channel 3 errors are much larger in the extratropics. While it is difficult to see here, channel 3 departures are typically larger near nadir due to surface sensitivity and seeing deeper into the troposphere ([Geer \*et al.\*, 2012](#)). This aids in down-weighting the other window channels for low zenith angles. For the sake of limiting the error model’s complexity, no additional zenith-based weighting of the errors is applied here, unlike for channel 5 in the operational implementation ([Duncan \*et al.\*, 2022](#), Fig. 3).

Using the relationship between  $\text{std}(\text{O-B})$  and  $C_{Ch3}$ , we can create a suitable error model for each channel as seen in Fig. 4 for channels 1, 2, and 15. The departures for channels 1 and 2 show a relatively linear increase with respect to the predictor but level off at higher values. Channel 15 departures increase steeply but level off very quickly, likely indicative of the cloud emission signal saturating. The error model assigns values larger than suggested by  $\text{std}(\text{O-B})$  alone for cloudy scenes, i.e. large  $C_{Ch3}$ ; this was done as earlier experimentation suggested benefits from down-weighting channel 15 in cloudy regions. The figure is split into extratropics (left) and tropics (right), and exemplifies the challenge of tuning a globally uniform error model, as the sensitivities change depending on environmental conditions such as columnar water vapour. For this reason, the error model is perhaps overly cautious in the extratropics, aiding to down-weight radiances in the more problematic southern ocean.

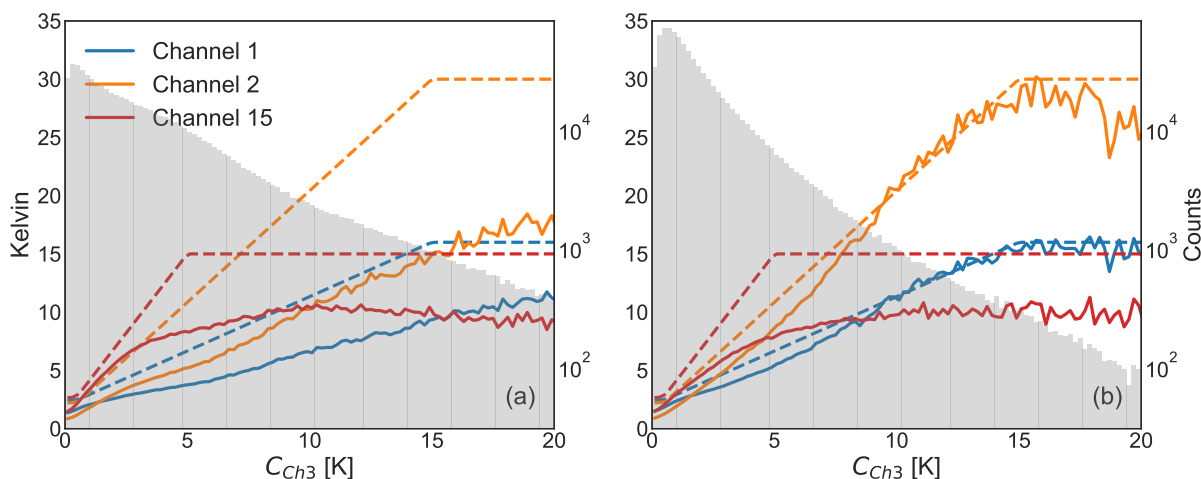


Figure 4: The channel 3-based error model for channels 1, 2, and 15 is shown (dashed lines) alongside  $\text{std}(\text{O-B})$  (solid lines) binned by  $C_{Ch3}$  value. Data are taken from a two-week period in December 2020 from all active AMSU-A sensors. On the left are data from the extratropics (a; latitudes greater than  $20^\circ$ ) and on the right are data from the tropics (b;  $20^\circ\text{S} < \text{latitude} < 20^\circ\text{N}$ ). Grey bars show the histogram of data counts per bin.

A key aspect for an optimal error model is that the resultant PDF of normalised departures is relatively Gaussian and unskewed. Figure 5 shows histograms of normalised departures using the three error models proposed above. Here all used observations over sea are given alongside “cloudy” ones, where cloud is defined in model space with either background or analysis column water path 0.2mm or greater (approximately a quarter of all observations). These plots also give similar GMI channels as a reference. The PDFs underscore the conservative nature of the error modelling as seen in the previous figure for

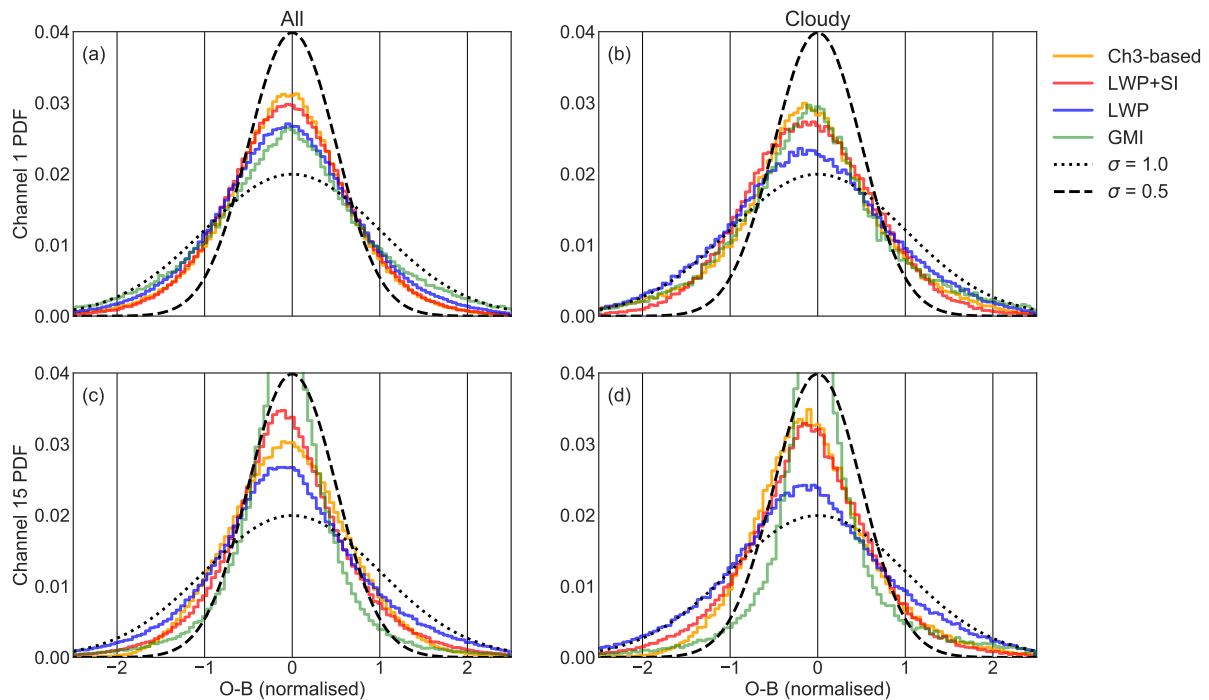


Figure 5: Channels 1 (a,b) and 15 (c,d) normalised background departure PDFs for all data (left) and cloudy data (right), comparing the Ch3-based, LWP+SI, and LWP-only error models. The nearest GMI channels (23.8 and 89 GHz vertically polarised) are shown for comparison. Statistics are from global used data over sea, December 15-19th 2020 from all AMSU-As together. Here “cloudy” is defined by model cloud for consistency, with combined water path in background or analysis greater than 0.2mm.

the Ch3-based model, namely that a majority of the radiances receive little weight in the assimilation due to large assigned errors. Such caution is preferable to over-weighting a biased PDF, exemplified by contrasting the cloudy channel 15 LWP-only and Ch3-based PDFs in panel (d). The slight negative bias of all-sky PDFs can be caused by insufficient atmospheric ice, too much liquid cloud, or too much column water vapour in the model (i.e. B is too large), if we neglect forward model errors.

The degree to which the normalised departure distribution is “peaked”, i.e. non-Gaussian, has long been an issue for all-sky assimilation (Geer and Bauer, 2011), and variational quality control is a method for taming this perhaps inherently peaked distribution in an NWP model (Bauer *et al.*, 2010), as discussed in Sec. 2.2. As shown in Fig. 5, given an almost identical sample of observations for AMSU-A window channels (shown for channels 1 and 15 only; channel 2 is similar to 1 but more conservative still), the choice of error model can mitigate certain elements of the bias or skew of the distribution of normalised departures. For instance, as seen for channel 15, the LWP-only model includes a significant population of global departures outside of -1-sigma errors, whereas the other error models do a better job of down-weighting these observations that often include significant atmospheric scattering; this is most apparent for the cloudy-only population (Fig. 5, right) where the LWP-only model is an outlier for heavily weighting negative O-Bs whereas the Ch3- and LWP+SI-based models are more conservative. It is interesting to note that while the Ch3- and LWP+SI-based models are conservative, they remain less so than that of the operational model for GMI 89V, which is more peaked for cloudy as well as all observations. To be clear, it is not immediately apparent that any of the examined error models is insufficient or overly optimistic at weighting, and analysis of the normalised PDFs of departures is not an exact science. However, it is plain from this figure that the Ch3- and LWP+SI-based error models help to better mimic the

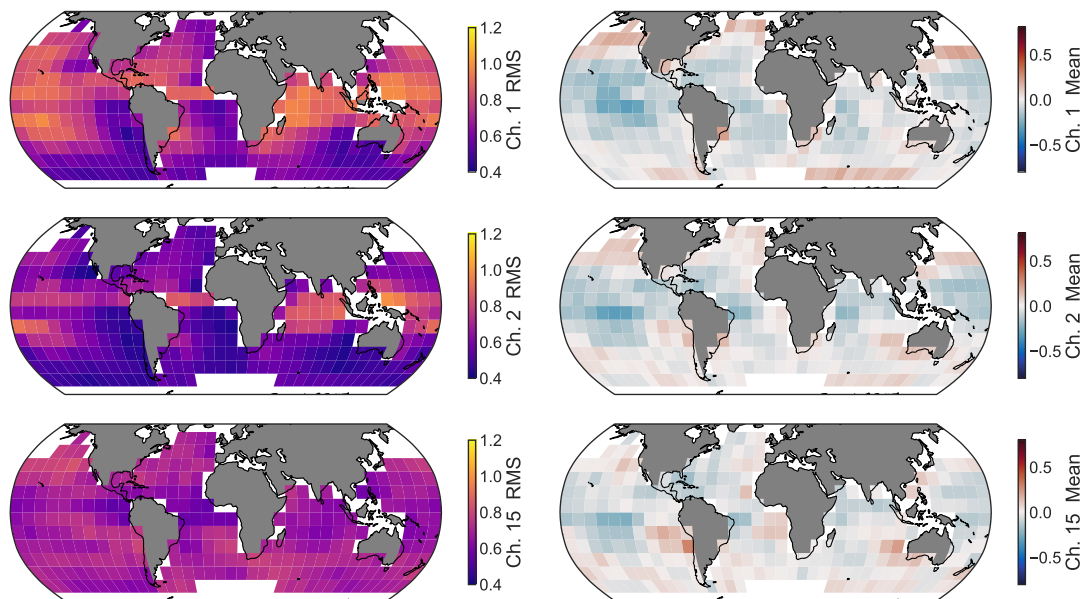


Figure 6: Maps of normalised background departures from December 2020 using the Ch3-based error model, with RMS on the left and mean on the right. Statistics are for used data only, averaged on a 10 degree grid. Any boxes with fewer than 5000 used radiances are in white, with land in grey.

error modelling characteristics of GMI that have proven successful in the operational model (Lean *et al.*, 2017). Moreover, while the PDFs for channels 1 and 15 are skewed, the Ch3-based error model appears to make the PDF less skewed, especially for the extremities of the normalised PDF.

Figures 6 and 7 provide maps of RMS and mean normalised background departures for December 2020. Comparison of the figures sheds some light on the relative positive and negative aspects of each error model. Each channel shows a slightly negative mean departure in much of the tropics and in the equatorial Pacific in particular. Net positive departures are found in channel 1 at high northern latitudes, perhaps indicating insufficient liquid water in modelled mid-latitude winter frontal clouds; net positive departures are also found in channels 2 and 15 off the coast of Chile and off the equatorial coast of west Africa, both common regions of stratocumulus cloud cover. In the maps of departure RMS, some significant differences are found between the error models. The relatively even RMS field for channel 15 when using the ch3-based model is notable here, whereas stratocumulus areas and the Southern Ocean show higher than desirable RMS values when using the LWP+SI model. In contrast, channels 1 and 2 show greater structure in the maps of RMS values when using the ch3-based model, with higher values in tropical regions of deep convection and precipitation.

To examine the geographical differences in weighting of observations, Fig. 8 shows the assigned observation errors for used channel 1 radiances over one assimilation cycle. Many small but important differences are visible in the weighting of the data. The channel 3 model assigns larger errors in less convectively active areas like the subtropical oceans and systematically assigns larger errors in the southern ocean; in addition, locations like the Black Sea, Gulf of Mexico, and Gulf Stream east of North America see larger errors, possibly indicative of surface effects. The LWP+SI model assigns larger errors in convective locations like the maritime continent and ultimately appears more binary (i.e. either on or off) than the more gradual channel 3 model.

A subtle but perhaps crucial advantage of channel 3 for observation error modelling is that all currently active AMSU-A sensors have a functioning channel 3. Thus a suitable error model can be applied across

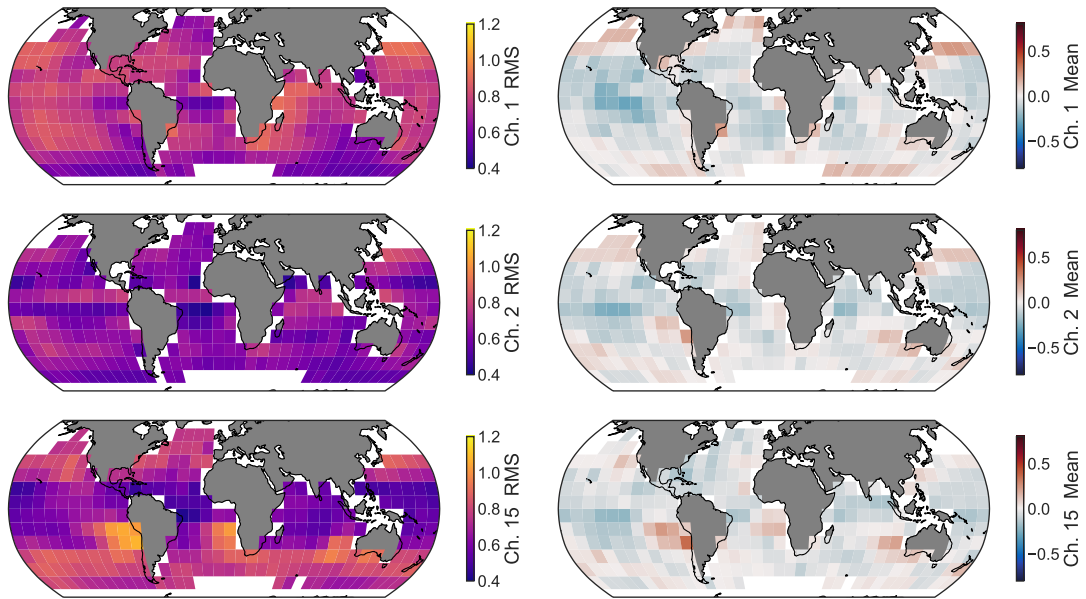


Figure 7: As Fig. 6 but using the LWP+SI error model.

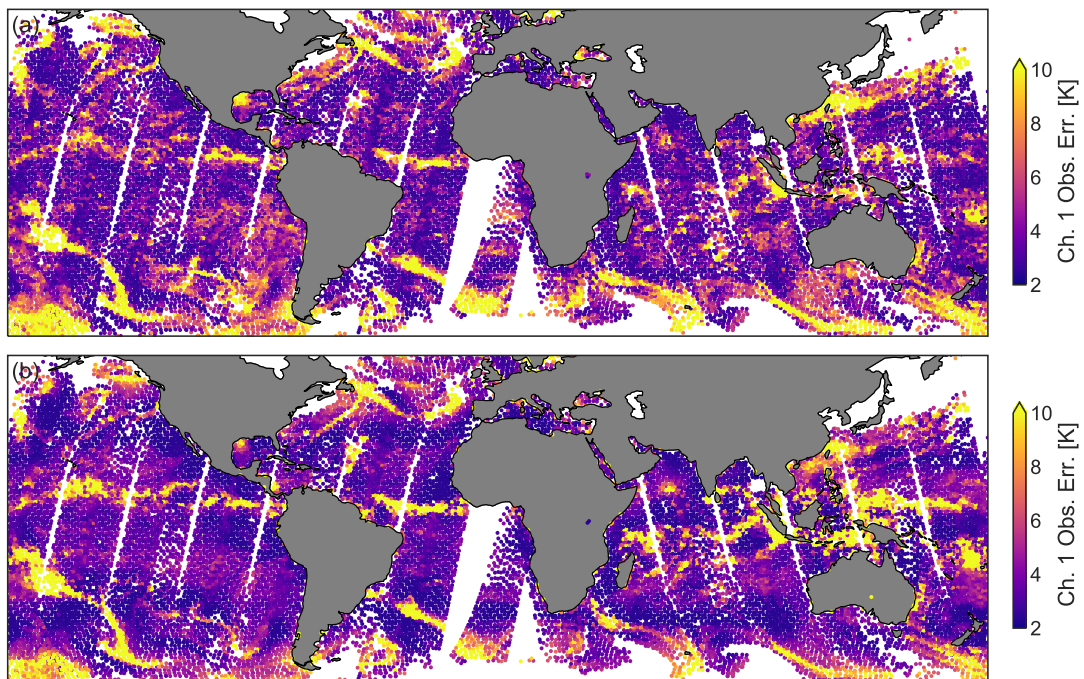


Figure 8: Assigned observation errors for (a) Ch3-based model and (b) LWP+SI model for channel 1 on Metop-A and -C for the 12Z analysis on 15th December 2020. Only assimilated observations are shown.

the board for all AMSU-A sensors. In contrast, solutions that involve channel 15 will exclude Metop-B window channels from use (see Table 3). That said, there is a large caveat when saying that channel 3 is “functioning” on all platforms, as the noise levels have been outside mission requirements for some time on all three Metop platforms. The clear-sky end of the error model is hence quite conservative, and especially so for sensors with high channel 3 noise. Despite performance outside original specifications, most cloud signals are several Kelvin and thus even a noisy channel 3 still suffices for most situations if the model is conservative.

## 2.2 Quality Control

As comprehensively detailed by Geer *et al.* (2022), the all-sky microwave developments for cycle 48r1 include several improvements for the treatment of surface-sensitive radiances over land, mixed scenes (combinations of sea-ice, water, and land), and high latitude oceans. There has also been a great deal of homogenisation for all-sky sensors in the IFS code that directly benefits the type of work presented here. Some of these “all-surface” developments are relevant for AMSU-A, but for its window channels specifically we remain cautious when it comes to screening and quality control. For instance, one advance in 48r1 is expanded use of window channels over high latitude ( $> 60^\circ$ ) oceans, but this is not applicable for AMSU-A as it lacks a 10GHz channel to check for fractional sea-ice. Hence, AMSU-A window channels retain screening for high latitudes and cold SSTs ( $< 274K$ ). 48r1 also assimilates 37GHz and 89GHz imager channels over land for the first time, albeit with large observation errors. It has not yet been tested whether AMSU-A channels 2 and 15 can be successfully assimilated over land—their greater surface sensitivity when viewing near nadir may make this more challenging, and it is outside the scope of this paper. Following the imagers, the regions of the Great Lakes and Caspian and Aral seas are explicitly screened out. Screening for AMSU-A window channels restricts their usage to ice-free oceans with land fraction less than 1%.

Variational quality control (VarQC) is a key element for all-sky radiance assimilation generally (Bauer *et al.*, 2010; Geer and Bauer, 2011), and activation of all-sky sounding channel radiances was no exception (Duncan *et al.*, 2022). For the window channels considered here, we follow the example of other all-sky window channels and prescribe an a priori probability of gross error of 0.5. This is larger than the probabilities assigned to sounding channels, which maximise at 0.2, but this is because the window channels are more prone to gross errors. No effort was made to tune VarQC a priori probabilities for the window channels considered here.

Figure 9 exemplifies the QC, showing departures from one long window analysis cycle—0Z on 15th June 2020. This depicts all observations from the Metop-B and -C platforms in the top panel and only QC'd observations that were used in the analysis on the bottom panel. Comparison of these two panels shows the cumulative effect of the quality control and screening procedures. Note the narrower swath due to screening of the three outside-most scan positions, data points screened out in the cold SSTs near Antarctica (i.e. cold sector screening (Forbes *et al.*, 2016; Lonitz and Geer, 2015)), coastal and inland water observations removed, and assorted large departures removed by VarQC or first-guess checks ( $> 3.0$  or  $> 3.5$  normalised departures removed, depending on channel). As is clearly visible in the southern ocean, the cold sector screening is particularly active in austral winter, with cold air masses originating in Antarctica removed due to their clear positive bias in the background.

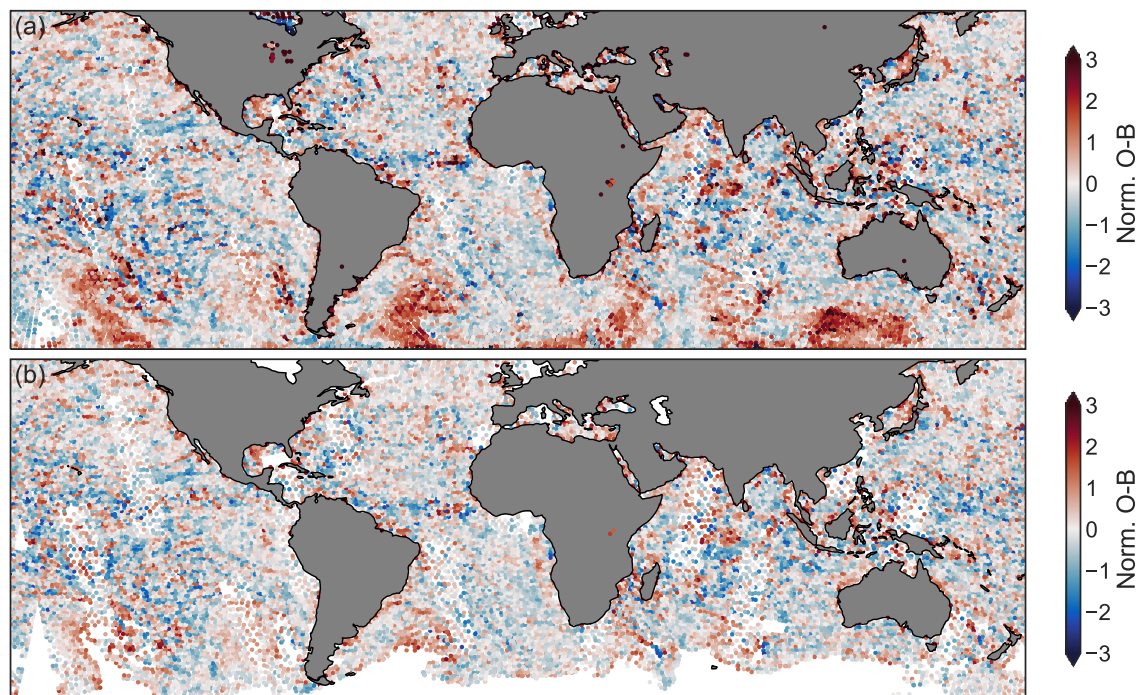


Figure 9: Normalised background departures from channel 1 on Metop-B and -C for the 0Z analysis on 15th June 2020. Panel (a) shows all observations (after thinning) over ocean, panel (b) contains only the observations that passed QC and affected the analysis.

### 2.3 Experimental Setup

The experiments in this paper use IFS cycle 47r3 (ECMWF, 2021) but contain every all-sky microwave enhancement included in the 48r1 upgrade as described by Geer *et al.* (2022). These include the “all-surface” elements for all-sky described therein, plus RTTOV-SCATT version 13 (Geer *et al.*, 2021), slant-path radiative transfer extended to humidity sounders (Bormann, 2017), and better treatment of ATMS radiances over snow (Bormann, 2021). The experiments discussed here all use the same version of the IFS and vary only in the microwave radiances that are actively assimilated and/or the way in which observation errors are modelled for the AMSU-A window channels. All experiments are run at TCo399 ( $\approx 27\text{km}$ ) final model resolution with 137 vertical levels.

One set of experiments uses a depleted observing system (relative to operations) to better isolate the signals from assimilating AMSU-A window channels (top half of Table 2). Here we remove all other window channels (18-91 GHz) from active use; this excludes data from SSMIS F17, GPM GMI, GCOM-W AMSR2, and FY-3D MWRI, forming the **Imagers Out** baseline experiment. From here we add in the AMSU-A window channels with different error models: LWP+SI, and Ch3-based. On the other end is **Imagers In**, with all 22 imager channels assimilated and no AMSU-A window channels, just as in current operations. The second set of experiments uses the full observational system (i.e. with imagers included) as the point of comparison (**Imagers In**).

The experiments each span two seasons. The summer season spans June to August 2020, and the winter season December 2020 to February 2021. During these time periods there were several AMSU-A sensors active in all-sky assimilation: Metop-A/B/C and NOAA-15/18/19. As mentioned earlier, Metop-B has had a broken channel 15 since 2016 and so its window channels are inactive in the LWP+SI experiment.

Table 2: Experiments are given by name and experiment ID, and have a description of which window channels are active. Note that AMSU-A here refers only to its window channels, with sounder channel usage (channels 5-14) unchanged in all experiments.

<i>Experiment</i>	<i>Exp ID(s)</i>	<i>Description</i>
<b>Imagers Out</b>	hnye/hpys	No window channels active
<b>+1/2/15 Ch3</b>	hnyf/hpyt	AMSU-A (Ch3 errors)
<b>+1/2/15 LWP+SI</b>	ho7t/hpyu	AMSU-A (LWP+SI errors)
<b>Imagers In</b>	hmpw/hmpx	Imagers only
<b>Imagers + 1/2/15 (Ch3)</b>	hnxx/hnxy	Imagers plus AMSU-A (Ch3 errors)
<b>Imagers + 1/2/15 (LWP+SI)</b>	hojo/hojp	Imagers plus AMSU-A (LWP+SI errors)

Table 3: Window channels on AMSU-A and on which satellites these channels were actively assimilated in the experimentation. Metop-B is given an asterisk because its broken channel 15 precludes its use with the LWP+SI model.

<b>Channel</b>	<b>Satellites where active</b>	<b>No. Active Ch3</b>	<b>No. Active LWP+SI</b>
<b>1</b>	Metop-A, -B*, -C, NOAA-15, -18, -19	6	5
<b>2</b>	Metop-A, -B*, -C, NOAA-18, -19	5	4
<b>15</b>	Metop-A, -C, NOAA-15, -18, -19	5	5

In addition, an asymmetric scan bias was discovered in NOAA-15 channel 2, causing exclusion of this channel from active use out of an abundance of caution. This means that from the six platforms together there are 16 window channels to assimilate during this time period<sup>1</sup>, with 16 used actively in the Ch3-based experiments and 14 in the LWP+SI experiments. The satellites and window channels assimilated are listed in Table 3.

### 3 Results

The results section is split in two, first to isolate the impact of window channel assimilation in experiments for which microwave imagers (18-91GHz) are denied entirely and then against the full set of observations used in operations. We assess the addition of AMSU-A window channels with both the Ch3-based (Eq. 6) error model and the LWP+SI (Eq. 5) error model, first in the depleted observing system and then the full system.

#### 3.1 Imagers denial

A comparison of forecast error changes between the denial experiments is found in Fig. 10. Tropical winds and TCWV are the parameters most improved by window channel assimilation. Changes in forecast skill in the extratropics are generally positive but dependent on the verification reference, as discussed below. It is encouraging that the main signals from imager assimilation such as improved short-to medium-range wind and TCWV scores are largely retained by the AMSU-A window channels in aggregate. The Ch3-based error model performs better with respect to forecast error reduction for tropical winds and TCWV, albeit not significantly so given the 6-month period studied.

<sup>1</sup>Metop-A de-orbited in November 2021, after the period of experimentation

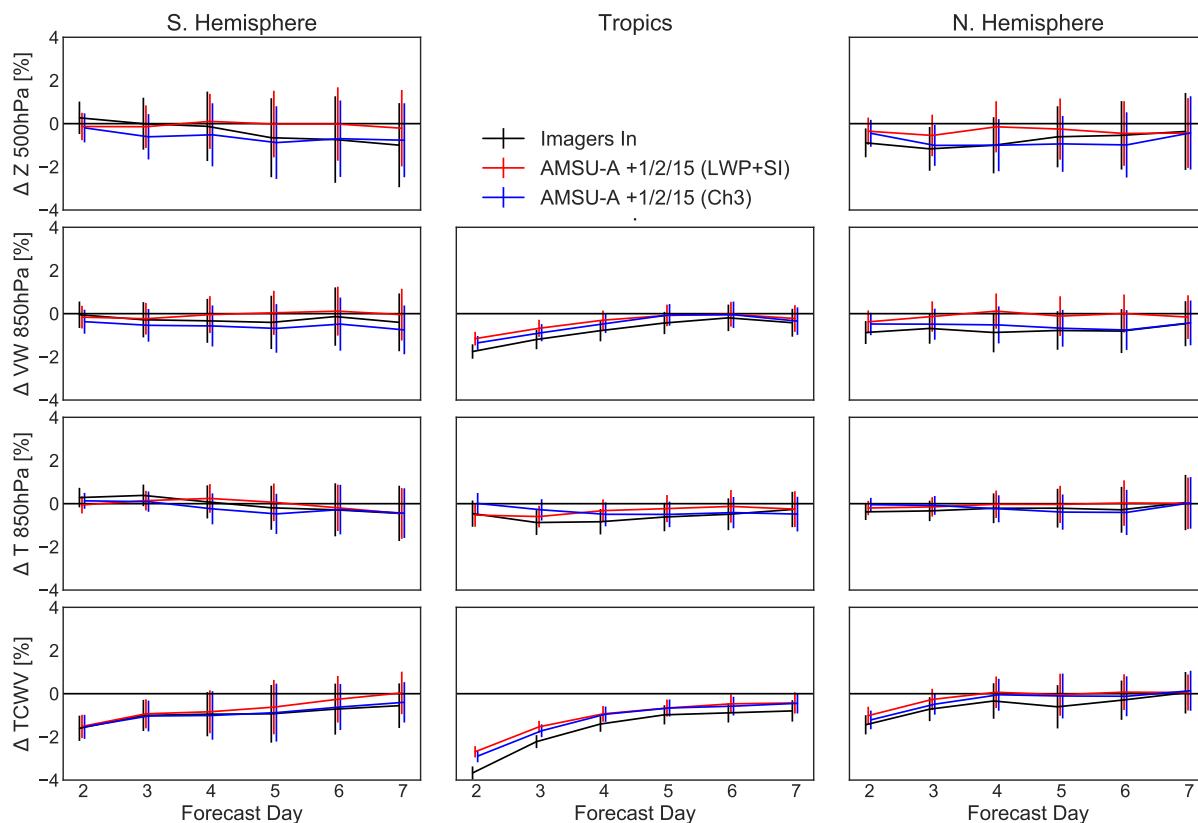


Figure 10: Changes in forecast RMSE relative to the depleted system (Imagers Out). Results are split into southern hemisphere extratropics (20S-90S; left), tropics (20S to 20N; centre), and northern hemisphere extratropics (20N-90N; right) for geopotential height (Z) at 500hPa, vector winds (VW) at 850hPa, temperature (T) at 850hPa, and total column water vapour (TCWV). Verification is against ECMWF operations.

One of the most salient impacts of all-sky microwave assimilation can be witnessed in wind forecasts at short ranges (e.g. Geer *et al.*, 2022; Duncan *et al.*, 2022). This is partially due to the sensitivity of microwave radiances to elements of the atmosphere that act as good wind tracers in 4D-Var (Peubey and McNally, 2009), namely water vapour at lower levels and moisture in clouds, but also a generalised 4D-Var tracing as seen in Bauer *et al.* (2010) and Geer *et al.* (2014). This impact on winds is clear in the imager denial experiments, shown in Fig. 11 verified against the operational analysis. Here the impact on winds from the imagers is seen side by side with the AMSU-A window channels, and the structures are very similar overall. Vector wind forecasts are improved by about 1% at low levels in the tropics but also northern mid-latitudes. The imagers addition causes apparent degradation of winds above Antarctica, though much of this is actually below the ground and not considered a large concern. Small improvements in mid-level wind forecasts at short ranges appear to persist in the tropics for a few days.

However, short-range verification is rather dependent on the verifying analysis. This can be seen comparing Fig. 11 with Fig. 12, with the latter using own-analysis verification. At 12 and 24hr lead times, the own-analysis verification gives a much more mixed picture of the impact of Imagers In and the window channel addition; the patterns for both become more consistent at 48 and 72hr lead times, with mid-level winds in the tropics convincingly improved. At these longer lead times where the verification reference is less important, the AMSU-A window channels' impact on wind forecasts compares favourably with that of the imagers. As short-range analysis verification is inherently unreliable (e.g. Bormann *et al.*,

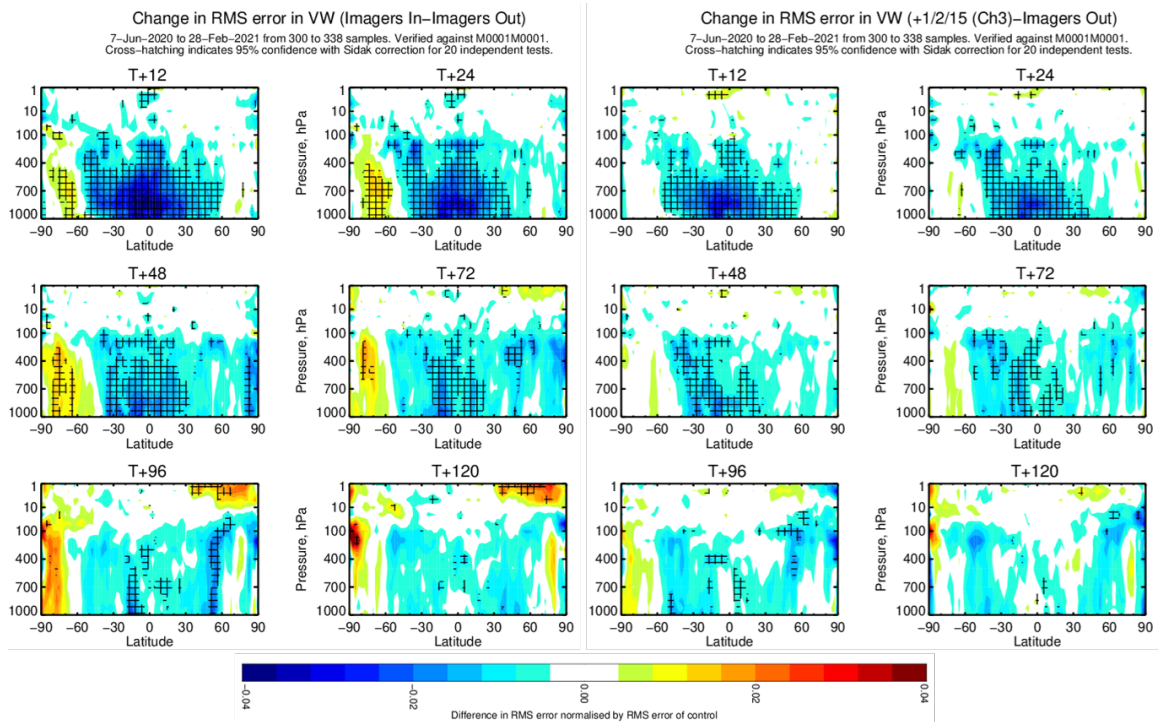


Figure 11: Changes in vector wind RMSE at forecast ranges from +12hr to +5 days, comparing forecast errors for the window channel assimilation relative to the depleted baseline. On the left is the result for Imagers In, on the right is using AMSU-A window channels with the Ch3-based error model. Verification is against operations.

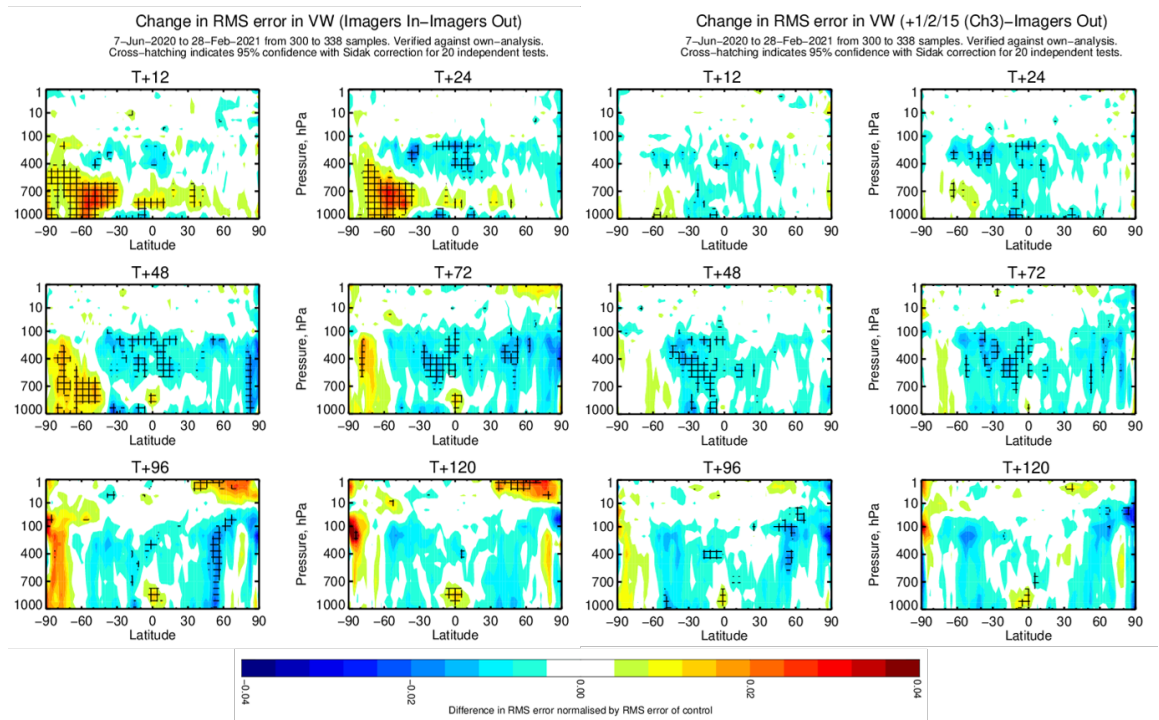


Figure 12: Same as previous figure but with own-analysis verification.

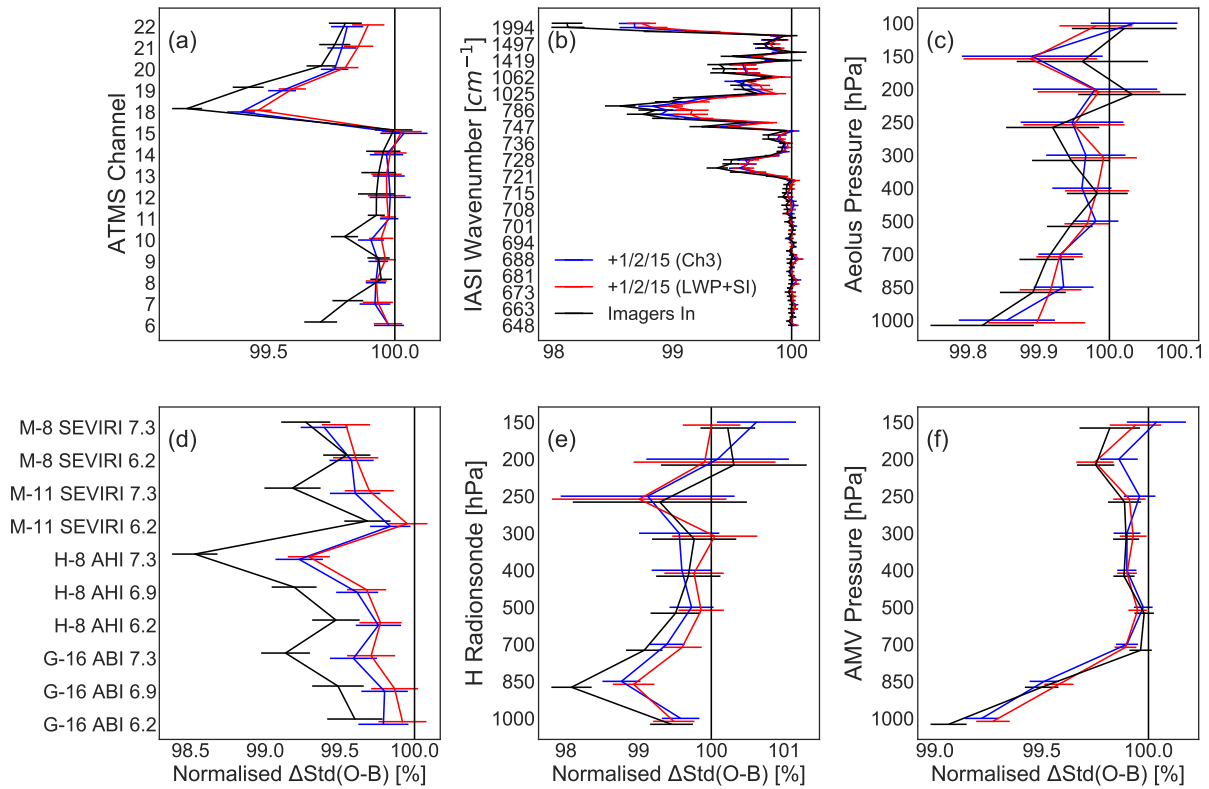


Figure 13: Changes in global background fits to other observations, as seen in: ATMS radiances (a), IASI radiances (b; Infrared Atmospheric Sounding Interferometer), Aeolus line-of-sight wind retrievals (c), geostationary infrared radiances (d; M=Meteosat, H=Himawari, G=GOES), humidity radionsondes (e), and AMVs (f; atmospheric motion vectors). The 100% line here represents the depleted system, i.e. Imagers Out. Only every fourth IASI channel is shown to aid interpretation.

2019), we turn to background fits to independent observations to better assess the short-range impacts.

Figure 13 shows the impact on background departures for other observation types. Whether using Eq. 6 or Eq. 5 for error modelling, the addition of AMSU-A window channels improves fits of the IFS to humidity-sensitive observations from radionsondes at low levels, IASI water vapour channels, and most markedly for geostationary infrared radiances. These results are in line with expectations, as microwave window channels are primarily a constraint on columnar atmospheric water vapour and hydrometeors. Improved fits to the ATMS humidity sounding channels are also notable for its lower peaking channels, 18 and 19, especially. There is not a large difference between the improvement seen from the Ch3-based error model and the LWP+SI model, though a slight advantage is apparent in several channels for the Ch3-based model. Regarding the wind impacts seen in analysis verification above, we can use AMV and Aeolus wind lidar retrievals (Rennie et al., 2021) to assess short-range impacts on winds. AMV observations (panel (f)) back up the positive winds impact for 12hr forecasts, with the levels at 850hPa and 1000hPa showing significant improvement due to AMSU-A window channel assimilation. Bolstering this evidence of wind impact, fits to Aeolus are improved in the lower troposphere, witnessed in panel (c). The winds impact is comparable to that of the imagers, similar to what was seen in Fig. 11.

These results in the depleted observing system demonstrate that window channel radiances from a sounder such as AMSU-A contain significant information on water vapour and winds that can be harnessed for global NWP with appropriate all-sky error modelling. Two distinct error models were tested

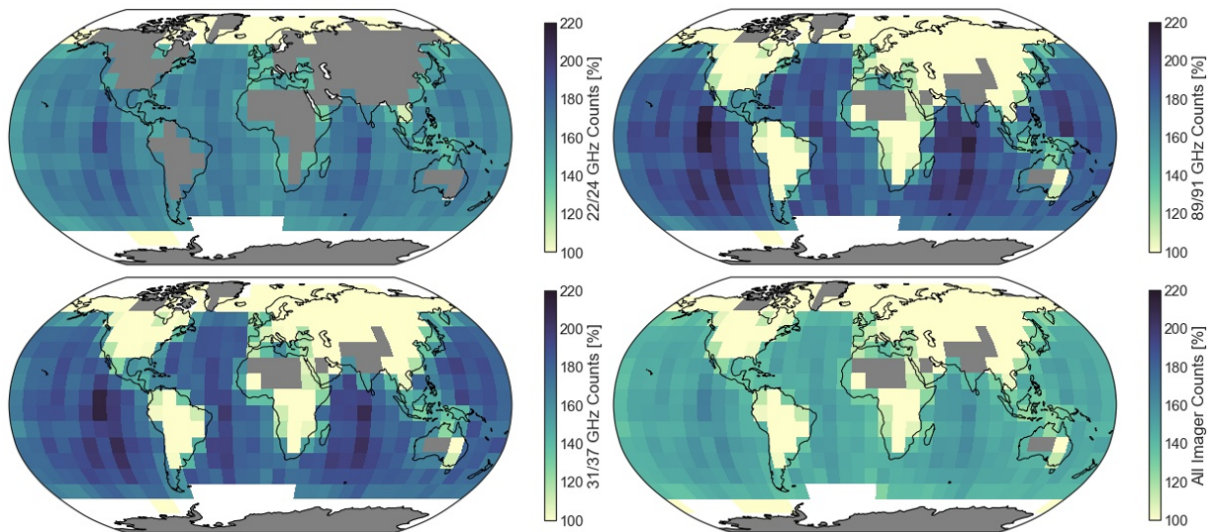


Figure 14: Maps showing window channel used data counts in the experiment with AMSU-A 1/2/15 active, normalised by the Imagers In counts. These are given for the three AMSU-A window frequencies and for all window channels (19-91 GHz) combined in the bottom right panel. Plots comprise used data July 1-10 2020, gridded at  $10^\circ$  resolution. Grey indicates land with no data counts; white indicates boxes with fewer than 500 counts.

here, with a slight edge given to the Ch3-based model in both fits to independent observations and forecast scores. Further comparison of the two error models is given in the following section for the full observing system.

## 3.2 Addition to full system

More pertinent to the possibility of future operational implementation, here we assess the impact of adding the AMSU-A window channels to a full system that includes four imagers, i.e. the operational 48r1 configuration. Figure 14 provides a sense of how much we increase the total number of observations assimilated for the three window frequency regions of AMSU-A channels 1, 2, and 15. There is a fairly uniform increase in the fraction of data added over ocean, but with slightly lower fractions of added data in high latitudes for reasons discussed in Sect. 2.2. Sampling increases are largest for AMSU-A channels 2 and 15 because these are imager frequencies where only one polarisation (i.e. V-pol) is assimilated.

### 3.2.1 Comparing error models in full system

To give more in-depth analysis of the performance of the two error models tested, here we examine the window channels added to the full observing system and compare the experiments head to head. The change in fits to independent observations are given in Fig. 15, with the blue lines representing the Ch3-based model in comparison to the LWP+SI model. This view makes it clear that short-range forecasts are better improved with the Ch3-based error model, better retaining positive impacts seen for low-level winds and fits to infrared and microwave humidity channels. An interesting result here is that the most improved fit for a microwave channel is at 150H on SSMIS, a channel somewhat like 50GHz in that it combines sounding and imager channel sensitivities. The relatively widespread agreement across observing systems confirms that the Ch3-based model has better performance than the LWP+SI model and that this likely goes beyond its advantage in permitting assimilation of Metop-B channels 1 and 2.

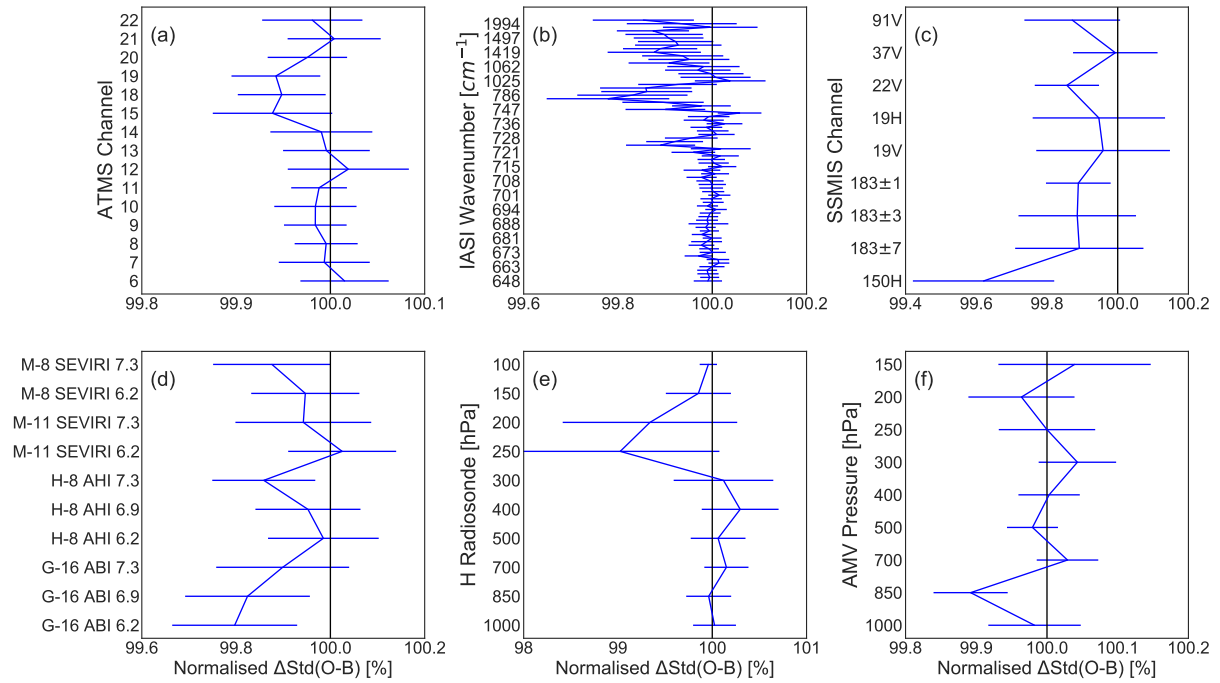


Figure 15: As Fig. 13, but here the 100% line is the LWP+SI experiment, with the blue lines the Ch3-based error model.

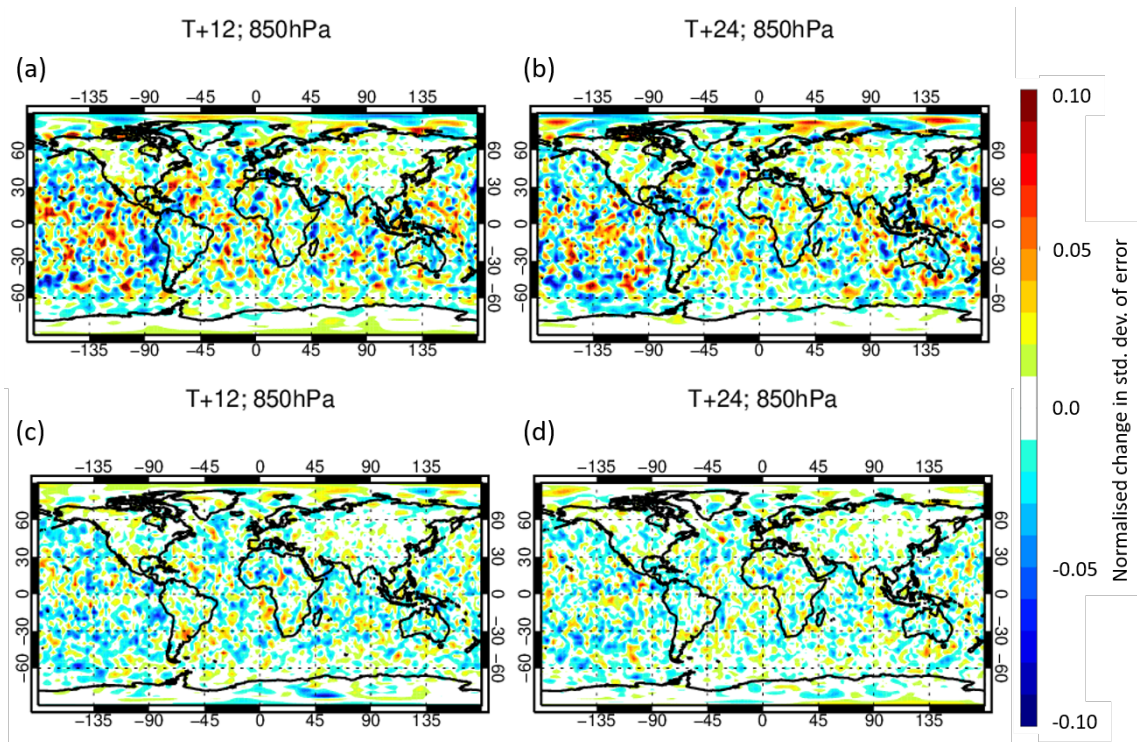


Figure 16: As Fig. 2, but here the comparison is Ch3-based minus LWP+SI forecast errors, i.e. blue areas show the Ch3-based model performs better than LWP+SI. Panels (a,b) are for temperature while panels (c,d) are for relative humidity.

One issue noted earlier, in reference to the LWP-only error model, was that degradation of low-level temperature and humidity was observed at short range (Fig. 2). Both error models tested improved this relative to the LWP-only model (not shown), but a good test of the models is which one better mitigates this adverse effect. Figure 16 provides this comparison again for temperature and humidity standard deviation at 850 hPa with the LWP+SI model as the reference. The areas of blue are relatively widespread in the humidity panels (c,d), indicating that the Ch3-based model performs better for low-level humidity verification at these short forecast ranges, with average performance almost 2% better for humidity in the tropics at T+12 when zonally averaged. The temperature plots (a,b) are noisier, but the southern hemisphere extratropics exhibit about 0.5% lower errors using the Ch3-based model (out to day 3), and there is a noticeable blue patch in the stratocumulus zone next to Chile, a problematic region for window channel assimilation. There is not a corresponding difference in the overall spatial standard deviation of these fields in the analysis, so these appear to be actual differences in the forecast verification. Further analysis of forecast scores is not presented in this section because almost none of the differences are significant, as one might expect given a relatively minor change to data usage and the 6-month time period of testing with a full observing system.

Bearing in mind the earlier results relative to the depleted system, these results allow us to conclude that the Ch3-based error model provides better forecast impact for the AMSU-A window channels when considered cumulatively. It permits inclusion of Metop-B window channels and mitigates some of the short-range degradations at high latitudes that are often problematic for all-sky radiance assimilation, yielding slightly better fits to independent observations overall. Hence we focus on the Ch3-based error model for the remainder of the report.

### 3.2.2 Comparison to full observing system

Changes in background fits to independent observations, as seen in Figs. 17 and 18, show the impact of window channel assimilation with Ch3-based errors for samples that are global and tropics-only, respectively. As seen in the experiments in the depleted system, the main impacts are visible in humidity-sensitive observations such as ATMS channels 18 and 19, and infrared water vapour channels such as on geostationary platforms and IASI. Fits to other assimilated microwave window channels such as those on SSMIS are much improved, a finding that is consistent across all imagers and most pronounced for the 23.8 GHz channels that primarily sense columnar water vapour. Comparing these two figures, again it is observed that improvements are largest in the tropics. AMVs show a nice improvement at low levels, consistent with the tracer effect from improved low-level moisture, however there is a small but significant degradation in AMV fits in the upper troposphere. Radio occultation (RO) measurements also indicate an improved fit for some tropospheric levels, whilst any signs of stratospheric degradation that can come from increased gravity waves due to all-sky assimilation are quite minimal, as seen in RO and ATMS stratospheric channels' (11-15) fits.

A striking feature of the fits to hyperspectral infrared radiances (IASI is shown here, but the same signal is seen for the Cross-track Infrared Spectrometer, CrIS) is the improvement seen for wavenumbers spanning about 750 to 1065  $cm^{-1}$ . These are infrared channels sensitive to the surface and atmospheric ozone, but also lower-tropospheric temperature and water vapour. Microwave window channel assimilation does not directly impact ozone or the surface, so this is a curious signal. Further analysis showed that used data counts for these wavenumbers were increased in the experiments where AMSU-A window channels were assimilated, so it is a doubly positive signal with increased data being assimilated and also a tighter fit to the background on average. This signal is strongest in the tropics, and is most striking in the middle of the Pacific where short-range TCWV forecasts are the most improved (not shown). Such a signal

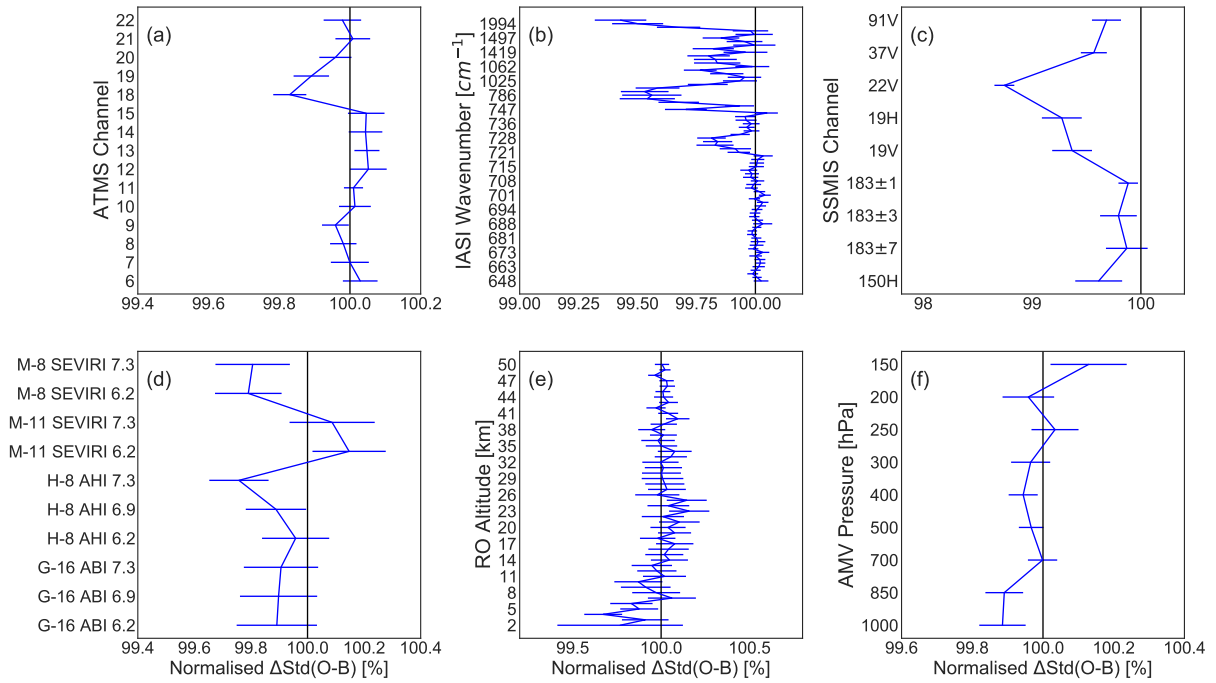


Figure 17: As Fig. 13, but with SSMIS radiances given in panel (c) and GNSS radio occultation in panel (e). Here the 100% line represents the full system, i.e. Imagers In, with the blue line denoting Imagers +1/2/15 (Ch3).

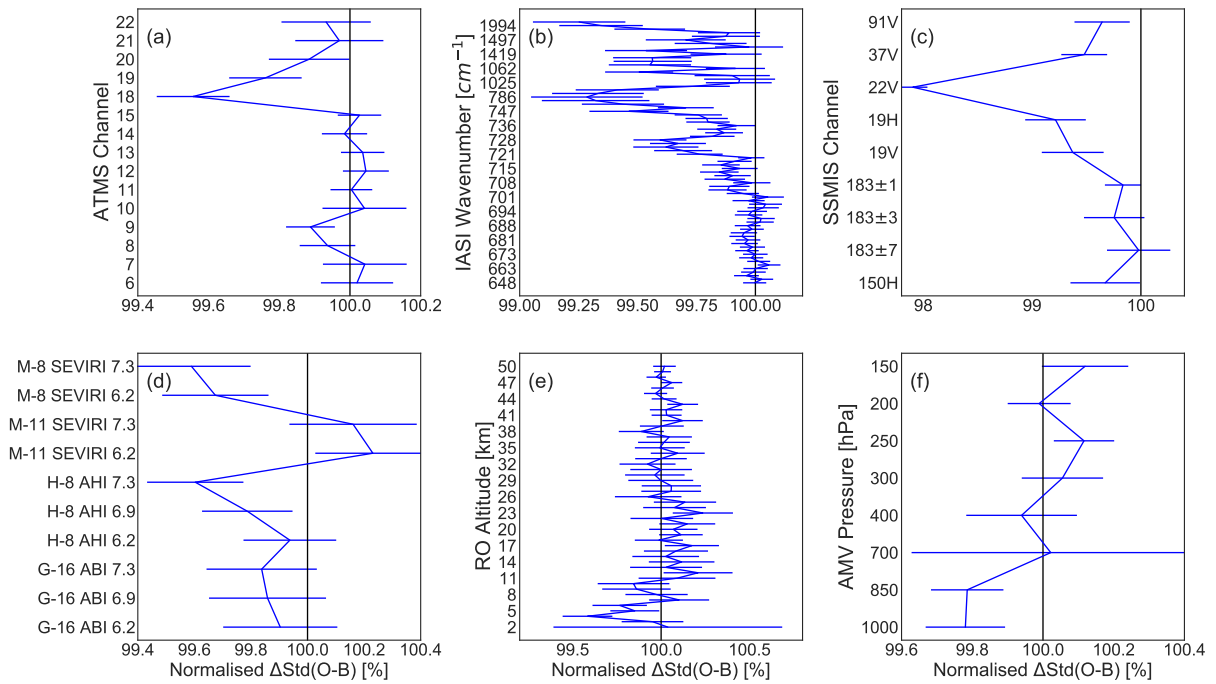


Figure 18: As Fig. 17 but considering observations in the tropics (20°S to 20°N) only.

is indicative of fewer radiances being rejected by the stringent cloud screening applied for low-peaking infrared channels, pointing to an improved moisture profile in the background (T. McNally, personal communication). This feature causes an increase of assimilated radiances from these IR channels that

is up to 7% in the tropics when comparing Imagers In against the depleted system. It accounts for a further increase of up to 1.5% in the tropics when AMSU-A window channels are assimilated, showing a positive synergy between infrared and microwave window channels in the IFS.

In Fig. 19 are shown the change in forecast RMSE for geopotential height at 500hPa, winds and temperature at 850hPa, and total column water vapour (TCWV). Verification against both own analysis and the operational analysis are shown to give context in light of Figs. 11 and 12. Some degradation is seen in southern hemisphere 850hPa temperature, and day 4 Z500 shows a 1% degradation that just passes the significance testing for the 95% confidence level following Geer (2016). There is an improvement at short range for TCWV, which is most apparent in the tropics but is nevertheless statistically significant in the extratropics through forecast day 2 when verifying against the operational analysis; it is a 0.5% improvement in the tropics at 1 day lead time with own-analysis verification and 1.5% for operational verification, so this appears to be a real signal at short range in the tropics. This improvement in TCWV is largest in the middle of the Pacific and the west Indian Ocean (not shown), which may reflect a small diurnal model bias being improved by greater window channel assimilation. The TCWV signal concurs with previous figures that reflect 12hr forecast improvements reflected in fits to observations, though much of this signal dissipates by day 2 and depends on verification reference. For most other forecast scores, the changes are relatively small and mostly neutral.

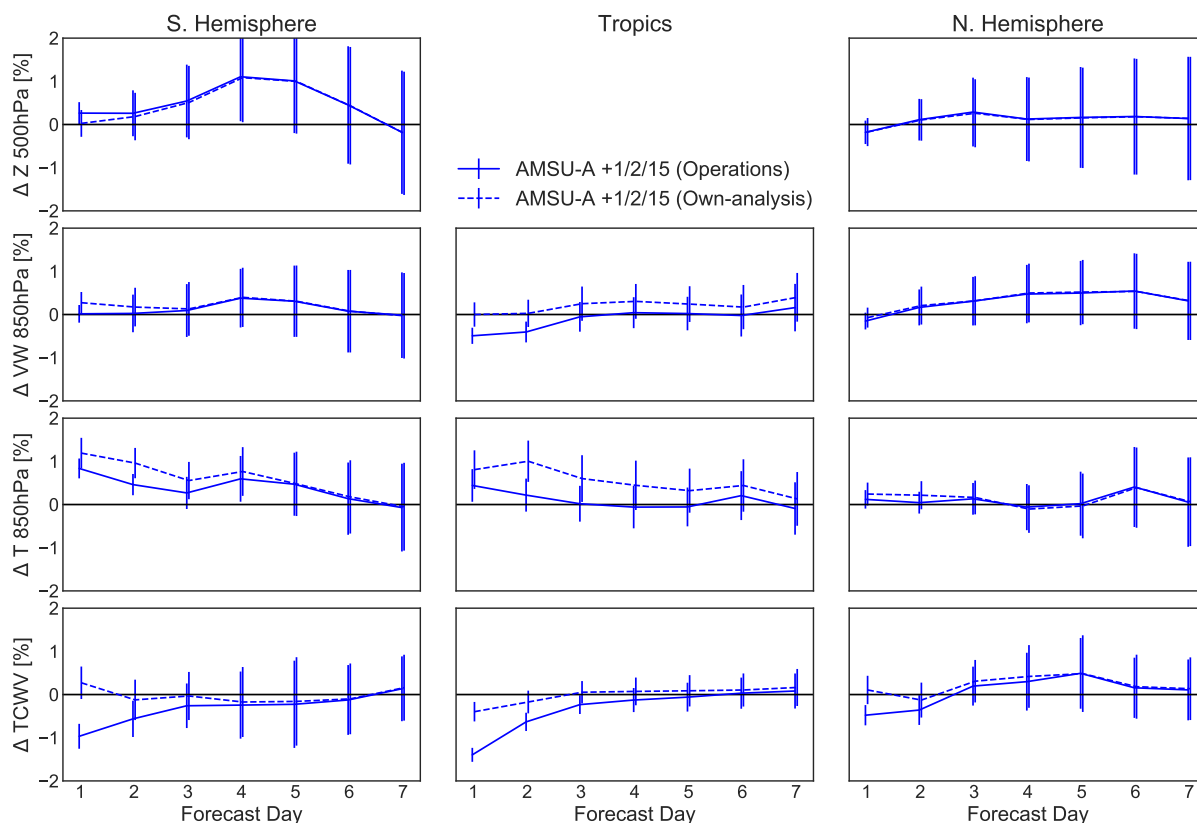


Figure 19: As Fig. 10 but relative to the full system (Imagers In) caused by assimilation of AMSU-A window channels. Verification is against ECMWF operations (solid) and own-analysis (dashed).

## 4 Conclusions

Expansion of microwave sounder assimilation beyond traditional sounding channels is in line with the all-sky and all-surface philosophy of microwave assimilation at ECMWF. These sensors' window channels hold valuable information on moisture and clouds that can be exploited through the framework of all-sky assimilation. In this report we have proven that the AMSU-A window channels at 23.8, 31.4, and 89 GHz do indeed possess similar information content as their counterpart channels on the conically-scanning imagers. Especially in an observing system with imagers absent, the benefit of AMSU-A window channel assimilation is very clear, with significant improvements to low-level moisture and winds. In fact, the overall impact approaches that of the four imagers combined in several respects.

Consideration of cross-track window channels caused probing questions to be asked about all-sky assimilation and the treatment of observation errors. It is not clear how an "optimal" all-sky error model should perform, nor how one error model should be evaluated against another. For previous sensors, the choice of error model was based upon a combination of availability (e.g. which channels or metrics were available) and physical intuition. In this paper we have evaluated two potential error models that are suitable for the window channels on a cross-track sensor; this list is of course not exhaustive, and further tuning could be investigated. The question of optimal error predictors is important for future all-sky assimilation, and is perhaps most salient for a sensor like ATMS (see Appendix A) that has several window channels and two suites of sounding channels. Furthermore, while we have considered observations over sea in this work, this question gains another dimension if we consider other surface types as well.

We conclude that the Ch3-based error model performed best for 1/2/15 assimilation over sea, as the results were marginally better for fits to other observations and reducing forecast errors. This was not, however, a clean comparison due to different treatment of Metop-B (see Table 3) and thus not definitive as to the performance of the models by themselves. Physical intuition suggests that some combination of the in-between frequency of channel 3 and its sensitivity to clear-sky errors from sources like the ocean skin temperature or low-level air temperature could be the key to this model's relative success. It is difficult to assess such causation quantitatively. Perhaps the key difference between the two models examined is the weight given to observations in the Southern Ocean and typical stratocumulus regions; this may be the main advantage of the Ch3-based error predictor, effectively down-weighting these regions that are historically problematic for all-sky radiance assimilation by using a predictor more sensitive to low-level liquid clouds.

It is unclear whether AMSU-A window channel assimilation as tested in this report should be considered for a future operational cycle. While the results in the depleted system are almost unambiguously positive and redolent of the imagers' overall impact, the results in the full observing system are more mixed. Background fits to observations point to an improved short-range forecast of low-level moisture and winds, particularly in the tropics. However, excepting TCWV at short ranges in the tropics, changes in forecast scores show little benefit and some small but persistent degradation of fields such as low-level temperature. Whether one views the AMSU-A window channels as a worthwhile addition to the operational system may rest on the relative importance of short-range fits to observations versus own-analysis forecast verification. As seen in early testing but not discussed here, limiting the use of window channels to +1/2 (i.e. excluding channel 15) might mitigate the degradations seen at low levels, and this will be tested with an eye to future implementation. Lastly, there is an argument to be made that the AMSU-A window channels could make the all-sky system more resilient in the case of data outages or newfound data quality issues with any of the imagers currently assimilated, but this is hard to quantify.

Several recent technical developments in the IFS have permitted this work on expanding the all-sky methodology to channels not previously considered for assimilation. Parallel to the work on AMSU-A

window channels, exploratory work on ATMS window channels and AMSU-A channel 4 is found in appendices [A](#) and [B](#). Briefly, we found that ATMS window channel assimilation broadly follows the results presented above and should be considered when moving ATMS to all-sky assimilation; channel 4 assimilation showed a more neutral impact. Although AMSU-A assimilation has been a fixture at ECMWF for over twenty years, it is clear that with further development and research it is possible to utilise previously discarded information to improve the overall assimilation. Such developments can continue to improve future weather forecasts through better use of heritage sensors, as demonstrated here, and there is a big potential benefit for reanalysis as well.

## A Appendix: ATMS window channels

ATMS is currently the sole passive microwave sensor assimilated in the IFS in clear-sky conditions only. The expectation is that its sounding channels will be moved to all-sky assimilation relatively soon, following the example of AMSU-A and MHS before that. Considering this expectation, it is appealing to apply the same window channel methodology of this report to the nearly identical window channels on ATMS for all-sky assimilation. Thus with an eye to the future, this trial is briefly described here. Ideally, when ATMS moves from clear-sky to all-sky assimilation it could be with almost every channel actively used from 23.8 to 190 GHz.

The first two channels on ATMS are identical to those on AMSU-A, with the same centre frequency and bandwidth. Channel 16 on ATMS is not quite identical to channel 15 on AMSU-A, with its centre frequency at 88.2 GHz (rather than 89.0) and a different bandwidth, but is considered equivalent for our purpose. Hence window channel assimilation trials for ATMS involve adding channels 1, 2, and 16 compared to AMSU-A 1, 2, and 15<sup>2</sup>. Because of the success of the AMSU-A channel 3 error predictor (Eq. 6), we adapt this for ATMS using the same frequency channel on this sensor, which is conveniently also named channel 3<sup>3</sup>. ATMS also holds a quasi-window channel at 165 GHz that could potentially be assimilated as well, but it is not considered here and would likely need a different error proxy.

The ATMS window channels were added in the IFS via all-sky assimilation, while leaving the clear-sky assimilation of the ATMS sounding channels unchanged. Aside from the all-sky vs clear-sky usage, two other aspects of the window-channel usage differ compared to that for the sounding channels. Firstly, the ATMS window channels are used unaveraged. For the clear-sky use of ATMS, channels are instead spatially averaged ((3x3 averaging, see [Bormann et al., 2013](#)), in order to reduce the sample noise. Low instrument noise is less crucial for window channels, and given the large FOV size of channels 1 and 2 spatial averaging is also not considered necessary to better match spatial scales represented in observations and the model background. Secondly, for the window channel assimilation discussed here, the outer six scan-positions on either side were removed from active use, whereas the full scan is used for the assimilation of the sounding channels. This is because initial trials showed large normalised departures for these scan positions for the window channels, possibly a result of emissivity model errors at high zenith angles, greater coastal contamination due to the very large footprint sizes, insufficient modelling of hydrometeors along the long slant path, or other factors. The maximum zenith angle used for ATMS window channels is hence approximately 55 degrees. These decisions on averaging and treatment of outer scan positions should be revisited in the future.

In contrast to the numerous AMSU-As, there are currently two ATMS sensors in operation: SNPP and NOAA-20 (with a third on NOAA-21 expected to launch later in 2022), and these cover the same orbital plane with an equator crossing time of 13:30. Thus activation of the ATMS window channels is expected to have a lesser impact with its six total window channels when compared to AMSU-A on six platforms during this time period.

Figure 20 shows the observation error model for ATMS channels 1, 2, and 16 over sea, giving the same view as Fig. 4. The error model is identical to that for AMSU-A and appears slightly more conservative for ATMS, but the overall picture is the same. There is certainly room for more fine tuning, particularly on the clear-sky end of the model.

---

<sup>2</sup>Whereas AMSU-A has a nadir footprint size of 48km for all channels, ATMS channels 1 and 2 have a 75km native footprint size while channel 16 has a 32km footprint.

<sup>3</sup>This channel on ATMS has quasi horizontal polarisation (QH), in contrast to vertical polarisation (QV) for channel 3 on AMSU-A

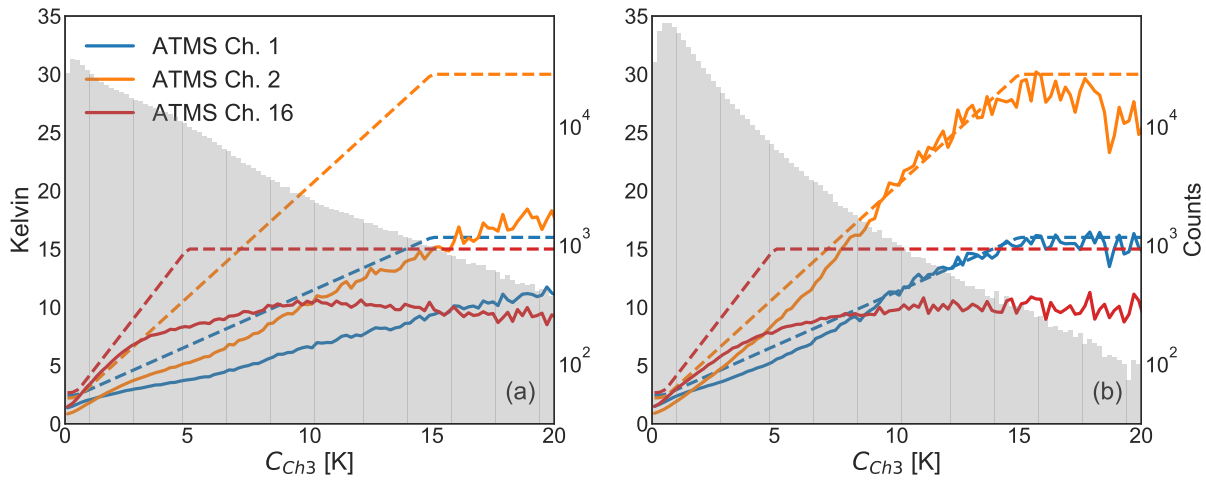


Figure 20: As Fig. 4 but for ATMS. Data from two week period, July 1-14, 2020.

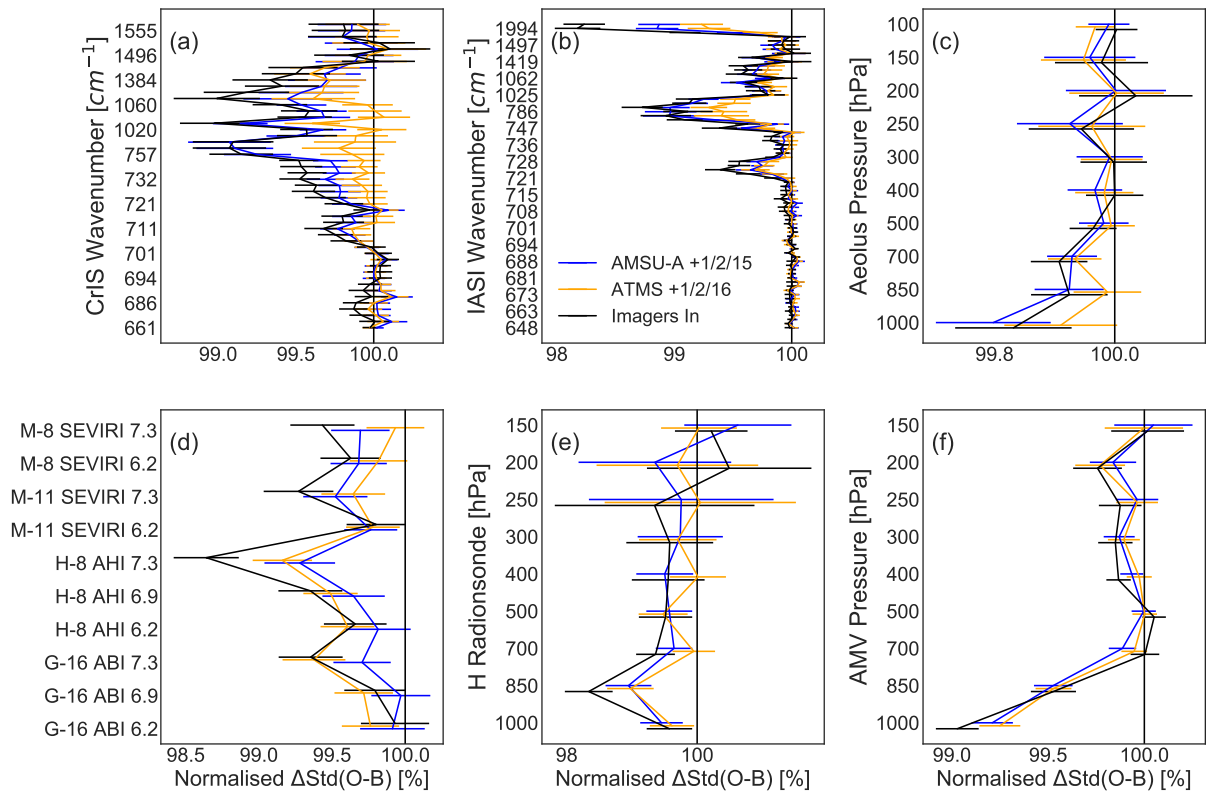


Figure 21: As Fig. 13, but comparing ATMS and AMSU-A window channel additions relative to the Imagers Out baseline. Here the Cross-track Infrared Spectrometer (CrIS) is given in panel (a) rather than ATMS temperature and humidity channels. The Imagers In statistics are given for reference.

To test the possibility of assimilating ATMS window channels, these were added to the depleted system as defined in Sec. 2.3 as Imagers Out. This methodology follows the idea that signals would be more apparent in the depleted system, and also allows comparison of the impact between ATMS and AMSU-A window channels cumulatively. Only one season (June to August 2020) was tested, and so we will focus on fits to other observations rather than forecast error changes. The change in fits to other observations are

given in Fig. 21. The impact on other observations is roughly similar to that from the AMSU-A window channel assimilation, which is a very encouraging result. Improved fits to lower tropospheric wind observations are seen for AMVs and Aeolus. Humidity-sensitive observations are similarly improved, seen across geostationary and polar-orbiting infrared radiances as well as a small but significant signal at 850hPa from radiosondes. The impact on CrIS and IASI radiances is overall smaller, but this is to be expected from the use of fewer total window channels as mentioned above.

This was a speculative experiment and as the assimilation of ATMS window channels has not been tested in the full observing system, it remains to be seen whether the impacts would follow those seen in this report, or indeed if combination of AMSU-A and ATMS window channels would work in synergy. At IFS Cycle 48r1 there has not yet been comprehensive testing of all-sky ATMS, but these encouraging results indicate that all-sky use of sounder window channels can and should be considered when testing future microwave sounders in the IFS, including upcoming sensors like MWTS-3.

## B Appendix: Channel 4

Channel 4 on AMSU-A is appealing for use in all-sky assimilation because it is frequently affected by cloud and precipitation due to its Jacobian peak of 920-810 hPa (Table 1) and its unique information on lower tropospheric temperature. For this reason it was considered one of the main reasons to move AMSU-A to all-sky assimilation originally (Geer *et al.*, 2012), as channel 4 was never operationally assimilated in the clear-sky stream at ECMWF. Furthermore, if AMSU-A window channels are assimilated, this remains the only channel other than channel 3 that is not actively used, whereas some other centres assimilate channel 4 in all-sky conditions already (Zhu *et al.*, 2016; Migliorini and Candy, 2019). All six AMSU-A sensors considered in this study have a working channel 4, and indeed all have very low ( $< 0.2K$ ) sensor noise levels. However, recent attempts to assimilate channel 4 in the IFS have had mixed results (Weston *et al.*, 2019) and the move to all-sky AMSU-A was thus for channels 5-14 only.

As with the window channels 1, 2, and 15, it is an open question which proxy is best for observation error modelling of channel 4. A LWP-only model may be appropriate, as tested previously by Geer *et al.* (2012) and Weston *et al.* (2019), but the greater sensitivity to the lower troposphere means that scattering from precipitation could also be an important error source and thus the LWP+SI model might perform better. The limited analysis here focuses on the LWP-only, LWP+SI, and Ch3-based models for a single season (June to August 2020) using the same depleted baseline of No Imagers used previously. Again this choice was made to better isolate signals from the channel activation.

Channel 4 is assimilated here over ocean and land, with the error model over land using SI alone—only the error model over sea differs between experiments. To isolate the effect of error model choice, Metop-B channel 4 is excluded from assimilation in all experiments. Building upon issues noted by Weston *et al.* (2019), two air-mass bias predictors (1000-300 and 200-50 hPa thickness) are added for channel 4 to bring its bias predictors closer in line with channel 5. Lastly, VarQC is set to 0.35 for channel 4, an a priori probability of gross error in between that of channel 5 (0.2) and the window channels (0.5). No modifications were made to the error models of channels 5-14.

Error model values are given in Table 4. The clear and cloudy proxy values differ between the LWP-based and Ch3-based models, with  $C_{clr,LWP} = 0.0$  and  $C_{cl,LWP} = 1.2$  versus  $C_{clr,Ch3} = 0.3$  and  $C_{cl,Ch3} = 15.0$ , with values in  $kgm^{-2}$  and K, respectively. Due to the substantially different noise performance of channel 3 on Metop and NOAA satellites, the clear-sky proxy and error values differ between the two sets, with proxies  $C_{clr,Ch3} = 0.3$  for NOAA and  $C_{clr,Ch3} = 0.6$  for Metop, and error values given in the table. These settings lead to similar numbers of used channel 4 radiances between the three experiments (within 1%),

Table 4: All-sky error model values are given for channel 4 on Metop and NOAA AMSU-A sensors. Each NOAA (15, 18, 19) and Metop (A, C) satellite is treated the same. All values given in Kelvin.

Satellite	Err. model	Clear (sea)	Cloudy (sea)	Clear (land)	Cloudy (land)
All	LWP-only	0.40	5.50	0.50	9.00
All	LWP+SI	0.40	5.50	0.50	9.00
NOAA	Ch3-based	0.35	3.50	0.50	9.00
Metop	Ch3-based	0.42	3.50	0.50	9.00

and the total number of channel 4 radiances assimilated being about 64% that of channel 5, a combination of Metop-B exclusion and quality control procedures.

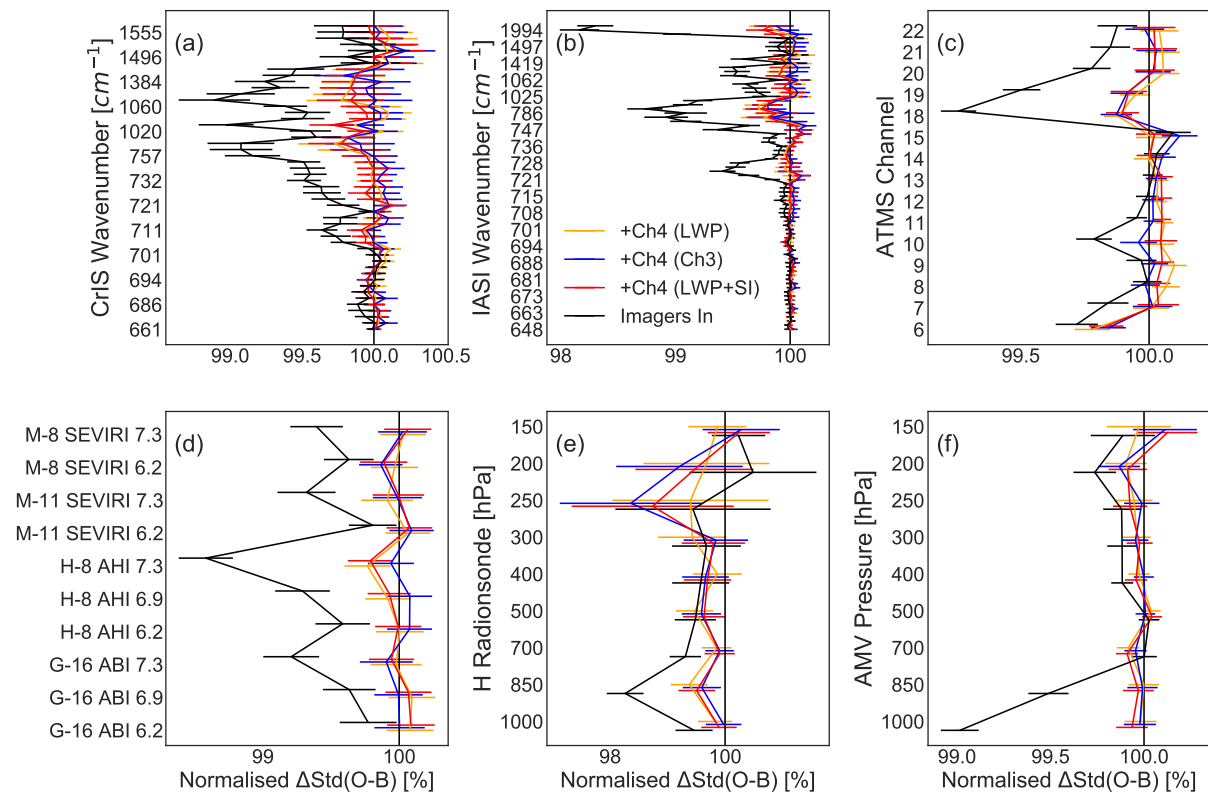


Figure 22: As Fig. 13, but for the addition of AMSU-A channel 4 with three different error models. Statistics are given for global data.

Results from channel 4 assimilation experiments using the three observation error models are given in Fig. 22, showing the change in background fits relative to No Imagers. For each of these observation types, it is hard to see much difference in performance between the three error models. There is some advantage evident from assimilating channel 4 regardless of the model used, with fits to radiosonde humidity improved by perhaps 0.5% in much of the troposphere and improved fits for the lowest-peaking ATMS humidity channels. Fits to AMVs and geostationary infrared are relatively neutral with slightly improved fits seen for some AMV levels, which could be considered a step forward relative to Weston *et al.* (2019, Fig. 17) albeit in a depleted system. These are noticeably more muted signals than those seen for the window channels combined, but are of course from one channel rather than three.

The addition of air-mass bias predictors removed the main structure of mean temperature increments

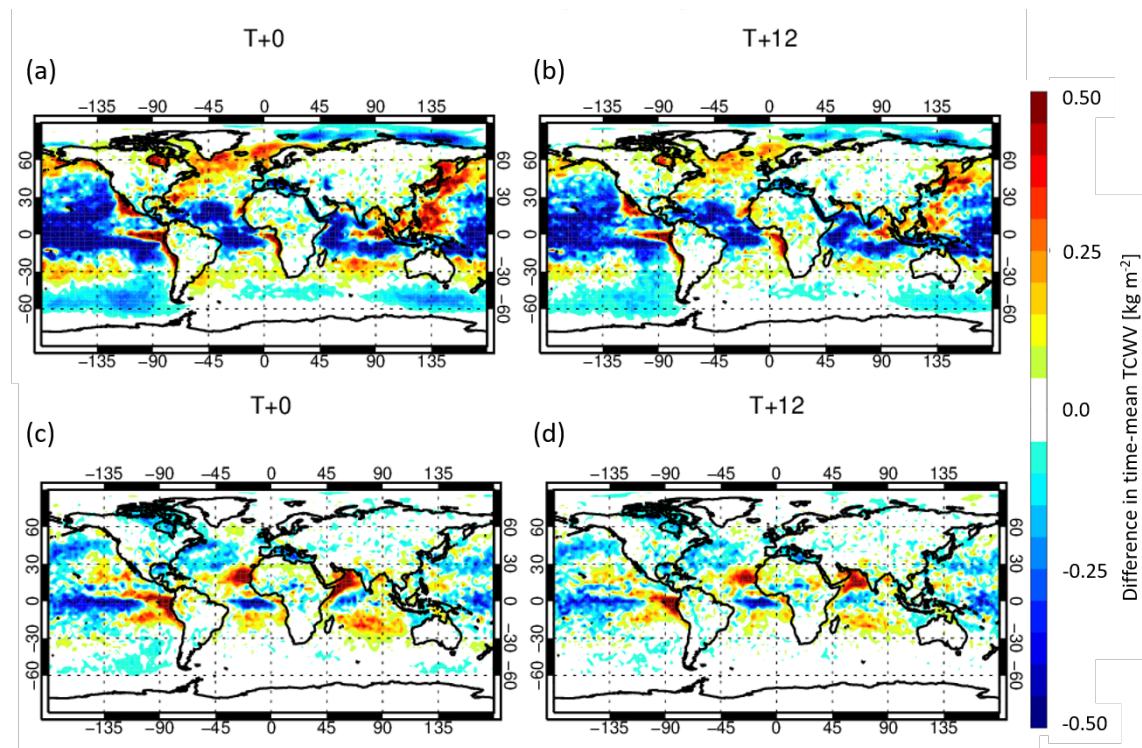


Figure 23: Difference in time-mean TCWV at forecast time +0 and +12hrs with respect to Imagers Out for Imagers In (a,b) and Ch4 (LWP+SI) (c,d).

noted by [Weston et al. \(2019\)](#), though as with the addition of the imagers, adding channel 4 causes some mean changes in the analysis such as weak cooling at 850hPa in the southern ocean, a mixture of changes in temperature and humidity at low levels in the tropics, and adding low cloud off the coast of Colombia (not shown). Perhaps most striking is the regional pattern of changes in the mean analysis of TCWV, with channel 4 showing a significant net effect on the mean analysis in the tropics. Figure 23 shows the mean change in the analysis and at +12hrs for TCWV, contrasting one of the channel 4 experiments (LWP+SI is shown, however the patterns are almost identical) against Imagers In. These signals weaken but persist from +12hrs through +48hrs in most regions, so it is not merely a transitory effect on the analysis. Notably, the mean shifts in analysed columnar water vapour show some areas of agreement between channel 4 and the imagers, such as along the equator in the Pacific Ocean, but also quite different signals in other regions, like west of Morocco and California or in the Arabian Sea. This figure demonstrates that although channel 4 and the imagers can pull the analysis through their sensitivity to low- and mid-level moisture, their sensitivities lead to differing impacts on the analysis via 4D-Var and appear to indicate independent information.

Looking at the previous two figures together, it is clear that channel 4 has a weaker influence on the analysis than the imagers, with impacts from channel 4 also much less than seen for the window channels combined in Fig. 13; indeed it is difficult to ascribe much impact from channel 4 on medium-range forecast scores even in the depleted setup used here. From this single season of experiments in a depleted system, we can conclude the following:

- The observation error model choice is of minor importance for channel 4 assimilation
- Channel 4 holds some unique information on humidity, particularly in the tropics

- Impact on the temperature analysis is relatively small, perhaps limited by the magnitude of clear-sky observation errors
- Although some benefit can be realised through assimilation of channel 4, it should not be considered a priority in the future

It may be possible to extract more impact from channel 4 by using tighter clear-sky errors, but this was not tested here. In the context of observation error model choices within this report, it mattered relatively little for channel 4, perhaps due to slightly higher-peaking sensitivity relative to the window channels or because channel 3 departures are too correlated for use with channel 4. It is also possible that much of the available signal from channel 4 is already supplied by channel 5, which uses relatively small clear-sky errors and less VarQC down-weighting while having a Jacobian that overlaps significantly; this is also a reasonable explanation why the all-sky AMSU-A implementation achieves greater FSOI for channel 5 but less for channel 6 when compared to clear-sky ([Duncan \*et al.\*, 2022](#), Table 5). Whatever the reason, despite several attempts at refining channel 4 assimilation and testing in a depleted system, it remains a challenge to realise significant benefit from addition of AMSU-A channel 4 radiances.

## Acknowledgements

The EUMETSAT Fellowship Programme supported David and has been instrumental in supporting the development of all-sky assimilation. David would like to thank Peter Weston for innumerable discussions that informed this work, and acknowledge the support of Stephen English and Andy Brown. Peter Lean and Mohamed Dahoui provided technical assistance. Thanks to Tony McNally for reviewing the manuscript.

## References

- Bauer, P., Geer, A. J., Lopez, P. and Salmond, D. (2010). Direct 4D-Var assimilation of all-sky radiances. Part I: Implementation. *Quart. J. Roy. Meteor. Soc.*, **136**(652), 1868–1885, doi:10.1002/qj.659, URL <https://rmets.onlinelibrary.wiley.com/doi/abs/10.1002/qj.659>.
- Blackwell, W. J., Braun, S., Bennartz, R., Velden, C., DeMaria, M., Atlas, R., Dunion, J., Marks, F., Rogers, R., Annane, B. and Leslie, R. V. (2018). An overview of the TROPICS NASA Earth venture mission. *Quart. J. Roy. Meteor. Soc.*, **144**(S1), 16–26, doi:10.1002/qj.3290, URL <https://rmets.onlinelibrary.wiley.com/doi/abs/10.1002/qj.3290>.
- Bormann, N. (2017). Slant path radiative transfer for the assimilation of sounder radiances. *Tellus A*, **69**(1), 1272779, doi:10.1080/16000870.2016.1272779, URL <https://doi.org/10.1080/16000870.2016.1272779>.
- Bormann, N. (2021). Investigating the use of Lambertian reflection in the assimilation of surface-sensitive microwave sounding radiances over snow and sea-ice. *Technical Report 886*, ECMWF Tech. Memo., Shinfield Park, Reading, doi:10.21957/hzcsrx8tt, URL <https://www.ecmwf.int/node/20180>.
- Bormann, N., Duncan, D., English, S., Healy, S., Lonitz, K., Chen, K., Lawrence, H. and Lu, Q. (2021). Growing operational use of FY-3 data in the ECMWF system. *Adv. Atmos. Sci.*, doi:10.1007/s00376-020-0207-3, URL <https://doi.org/10.1007/s00376-020-0207-3>.
- Bormann, N., Fouilloux, A. and Bell, W. (2013). Evaluation and assimilation of ATMS data in the ECMWF system. *J. Geophys. Res. Atmos.*, **118**(23), 12,970–12,980, doi:10.1002/2013JD020325, URL <https://agupubs.onlinelibrary.wiley.com/doi/abs/10.1002/2013JD020325>.
- Bormann, N., Geer, A. J. and Bauer, P. (2011). Estimates of observation-error characteristics in clear and cloudy regions for microwave imager radiances from numerical weather prediction. *Quart. J. Roy. Meteor. Soc.*, **137**(661), 2014–2023, doi:10.1002/qj.833.
- Bormann, N., Lawrence, H. and Farnan, J. (2019). Global observing system experiments in the ECMWF assimilation system. *Technical Report 839*, ECMWF Tech. Memo., doi:10.21957/sr184iyz, URL <https://www.ecmwf.int/node/18859>.
- Duncan, D. I., Bormann, N., Geer, A. J. and Weston, P. (2022). Assimilation of AMSU-A in all-sky conditions. *Mon. Weather Rev.*, **150**(5), 1023 – 1041, doi:10.1175/MWR-D-21-0273.1, URL <https://doi.org/10.1175/MWR-D-21-0273.1>.
- Duncan, D. I., Bormann, N. and Hólm, E. (2021). On the addition of microwave sounders and numerical weather prediction skill. *Quart. J. Roy. Meteor. Soc.*, **147**(740), 3703–3718, doi:10.1002/qj.4149, URL <https://doi.org/10.1002/qj.4149>.
- Duncan, D. I., Kummerow, C. D., Dolan, B. and Petković, V. (2018). Towards variational retrieval of warm rain from passive microwave observations. *Atmos. Meas. Tech.*, **11**(7), 4389–4411, doi:10.5194/amt-11-4389-2018, URL <https://www.atmos-meas-tech.net/11/4389/2018/>.
- ECMWF (2021). *IFS Documentation CY47R3 - Part II: Data assimilation*. Number 2 in IFS Documentation, ECMWF, doi:10.21957/t445u8kna, URL <https://www.ecmwf.int/node/20196>.

- Forbes, R., Geer, A. J., Lonitz, K. and Ahlgrimm, M. (2016). Reducing systematic errors in cold-air outbreaks. *ECMWF Newsletter*, pp. 17–22, doi:10.21957/s41h7q7l, URL <https://www.ecmwf.int/node/17261>.
- Geer, A. J. (2016). Significance of changes in medium-range forecast scores. *Tellus A*, **68**(1), 30229, doi:10.3402/tellusa.v68.30229, URL <https://doi.org/10.3402/tellusa.v68.30229>.
- Geer, A. J., Baordo, F., Bormann, N. and English, S. (2014). All-sky assimilation of microwave humidity sounders. *Technical Report 741*, ECMWF Tech. Memo., doi:10.21957/obosmx154, URL <https://www.ecmwf.int/node/9507>.
- Geer, A. J. and Bauer, P. (2011). Observation errors in all-sky data assimilation. *Quart. J. Roy. Meteor. Soc.*, **137**(661), 2024–2037, doi:10.1002/qj.830, URL <https://rmets.onlinelibrary.wiley.com/doi/abs/10.1002/qj.830>.
- Geer, A. J., Bauer, P. and English, S. (2012). Assimilating AMSU-A temperature sounding channels in the presence of cloud and precipitation. *Technical Report 24*, EUMETSAT/ECMWF Fellowship Programme Research Report, URL <https://www.ecmwf.int/node/9513>, also published as ECMWF Technical Memorandum 670.
- Geer, A. J., Bauer, P., Lonitz, K., Barlakas, V., Eriksson, P., Mendrok, J., Doherty, A., Hocking, J. and Chambon, P. (2021). Bulk hydrometeor optical properties for microwave and sub-millimetre radiative transfer in RTTOV-SCATT v13.0. *Geosci. Model Dev.*, **14**(12), 7497–7526, doi:10.5194/gmd-14-7497-2021, URL <https://gmd.copernicus.org/articles/14/7497/2021/>.
- Geer, A. J., Lonitz, K., Duncan, D. I. and Bormann, N. (2022). Improved surface treatment for all-sky microwave observations. *Technical Report 894*, ECMWF Tech. Memo., Shinfield Park, Reading, doi:10.21957/zi7q6hau, URL <https://www.ecmwf.int/node/20337>.
- Grody, N., Zhao, J., Ferraro, R., Weng, F. and Boers, R. (2001). Determination of precipitable water and cloud liquid water over oceans from the NOAA 15 advanced microwave sounding unit. *J. Geophys. Res. Atmos.*, **106**(D3), 2943–2953, doi:10.1029/2000JD900616, URL <https://agupubs.onlinelibrary.wiley.com/doi/abs/10.1029/2000JD900616>.
- Lean, K., Bormann, N. and Healy, S. (2022). Calibration of EDA spread and adaptation of the observation error model. *Technical Report WP-2000*, ECMWF, doi:10.21957/1auh0nztg, URL <https://www.ecmwf.int/node/20302>.
- Lean, P., Geer, A. and Lonitz, K. (2017). Assimilation of Global Precipitation Mission (GPM) Microwave Imager (GMI) in all-sky conditions. *Technical Report 799*, ECMWF Tech. Memo., doi:10.21957/8orc7sn33, URL <https://www.ecmwf.int/node/17174>.
- Lonitz, K. and Geer, A. J. (2015). New screening of cold-air outbreak regions used in 4D-Var all-sky assimilation. *Technical Report 35*, EUMETSAT/ECMWF Fellowship Programme Research Report, Shinfield Park, Reading, URL <https://www.ecmwf.int/node/10777>.
- Lonitz, K. and Geer, A. J. (2017). Effect of assimilating microwave imager observations in the presence of a model bias in marine stratocumulus. *Technical Report 44*, EUMETSAT/ECMWF Fellowship Programme Research Report, Shinfield Park, Reading, URL <https://www.ecmwf.int/node/10777>.

- Lonitz, K. and Geer, A. J. (2020). Reducing the drying effect through a water vapour correction to the all-sky error model. *Technical Report 53*, EUMETSAT/ECMWF Fellowship Programme Research Report, doi:10.21957/qmy8utbgb, URL <https://www.ecmwf.int/node/19528>.
- Migliorini, S. and Candy, B. (2019). All-sky satellite data assimilation of microwave temperature sounding channels at the Met Office. *Quart. J. Roy. Meteor. Soc.*, **145**(719), 867–883, doi:10.1002/qj.3470, URL <https://rmets.onlinelibrary.wiley.com/doi/abs/10.1002/qj.3470>.
- Peubey, C. and McNally, A. (2009). Characterization of the impact of geostationary clear-sky radiances on wind analyses in a 4D-Var context. *Quart. J. Roy. Meteor. Soc.*, **135**(644), 1863–1876, doi:10.1002/qj.500, URL <https://rmets.onlinelibrary.wiley.com/doi/abs/10.1002/qj.500>.
- Rennie, M. P., Isaksen, L., Weiler, F., de Kloe, J., Kanitz, T. and Reitebuch, O. (2021). The impact of aolus wind retrievals on ECMWF global weather forecasts. *Quart. J. Roy. Meteor. Soc.*, **147**(740), 3555–3586, doi:<https://doi.org/10.1002/qj.4142>, URL <https://rmets.onlinelibrary.wiley.com/doi/abs/10.1002/qj.4142>.
- Schulte, R. M. and Kummerow, C. D. (2019). An optimal estimation retrieval algorithm for microwave humidity sounding channels with minimal scan position bias. *J. Atmos. Oceanic Technol.*, **36**(3), 409 – 425, doi:10.1175/JTECH-D-18-0133.1, URL <https://journals.ametsoc.org/view/journals/atot/36/3/jtech-d-18-0133.1.xml>.
- Weston, P. and Bormann, N. (2018). Enhancements to the assimilation of ATMS at ECMWF: Observation error update and addition of NOAA-20. *Technical Report 48*, EUMETSAT/ECMWF Fellowship Programme Research Report, URL <https://www.ecmwf.int/node/18744>.
- Weston, P., Geer, A. J. and Bormann, N. (2019). Investigations into the assimilation of AMSU-A in the presence of cloud and precipitation. *Technical Report 50*, EUMETSAT/ECMWF Fellowship Programme Research Report, doi:10.21957/ewahn9ce, URL <https://www.ecmwf.int/node/19221>.
- Zhu, Y., Gayno, G., Purser, R. J., Su, X. and Yang, R. (2019). Expansion of the all-sky radiance assimilation to ATMS at NCEP. *Mon. Weather Rev.*, **147**(7), 2603–2620, doi:10.1175/MWR-D-18-0228.1, URL <https://doi.org/10.1175/MWR-D-18-0228.1>.
- Zhu, Y., Liu, E., Mahajan, R., Thomas, C., Groff, D., Delst, P. V., Collard, A., Kleist, D., Treadon, R. and Derber, J. C. (2016). All-sky microwave radiance assimilation in NCEP’s GSI analysis system. *Mon. Weather Rev.*, **144**(12), 4709 – 4735, doi:10.1175/MWR-D-15-0445.1, URL <https://journals.ametsoc.org/view/journals/mwre/144/12/mwr-d-15-0445.1.xml>.